Article:
Reinhard, AA, Jackson, MG, Koornneef, JM et al. (6 more authors) (2018) Sr and Nd isotopic compositions of individual olivine-hosted melt inclusions from Hawai'i and Samoa: Implications for the origin of isotopic heterogeneity in melt inclusions from OIB lavas. Chemical Geology, 495. pp. 36-49. ISSN 0009-2541

https://doi.org/10.1016/j.chemgeo.2018.07.034

Sr and Nd isotopic compositions of individual olivine-hosted melt inclusions from Hawaii and Samoa: implications for the origin of isotopic heterogeneity in melt inclusions from OIB lavas

A.A. Reinhard[1], M.G. Jackson[1], J.M. Koornneef [2], E.F. Rose-Koga[3], J. Blusztajn[4], J.G. Konter[5], K.T. Koga[3], P. J. Wallace[6], J. Harvey[7]

[1] University of Calfornia Santa Barbara, Department of Earth Science, Santa Barbara, CA, (reinhard@umail.ucsb.edu)

[2] Vrije Universiteit Amsterdam, Faculty of Science, Amsterdam, NL

[3] Universite Blaise Pascal, CNRS, IRD Laboratoire Magmas et Volcans, OPGC, Clermont-Ferrand, FR

[4] Woods Hole Oceanographic Institution, Woods Hole, MA

[5]University of Hawaii Manoa, Department of Geology and Geophysics, Honolulu, HI

[6] University of Oregon, Department of Earth Science, Eugene, OR

[7]University of Leeds, School of Earth and Environment, Leeds, UK

ABSTRACT

Geochemical investigations of mantle heterogeneity as sampled by ocean island basalts (OIB) have long relied on isotopic analyses of whole rock lavas. However, recent work has shown that significant isotopic disequilibrium can exist between the phases (groundmass and phenocrysts) of a single OIB lava. In this study, we target individual olivine hosted melt inclusions from two lavas—one Samoan and one Hawaiian—with melt inclusion $^{87}Sr/^{86}Sr$ heterogeneity previously observed using laser ablation inductively coupled plasma mass spectrometry (LA-ICP-MS). We report $^{87}Sr/^{86}Sr$ and $^{143}Nd/^{144}Nd$ in individual melt inclusions using thermal ionization mass spectrometry (TIMS). In melt inclusions from Samoan sample AVON3-71-2, we find highly heterogeneous (935 ppm) $^{87}Sr/^{86}Sr$ (0.705193 – 0.705853, N=6), consistent with previously identified $^{87}Sr/^{86}Sr$ heterogeneity (~2030 ppm) by laser ablation multi-collector ICP-MS (0.70459 – 0.70602, N=12). In contrast, we find very little (251 ppm) $^{87}Sr/^{86}Sr$

heterogeneity (0.703761 – 0.703938, N=9) in olivine hosted melt inclusions of a Hawaiian scoria from the Puu Wahi eruption (Mauna Loa), which contrasts with a prior observation which used laser ablation single-collector ICP-MS and found highly heterogeneous (~8500 ppm) $^{87}Sr/^{86}Sr$ in olivine-hosted melt inclusions from the same eruption (0.7021 – 0.7081, N=137). In both the AVON3-71-2 and Puu Wahi melt inclusions, the $^{143}Nd/^{144}Nd$ is indistinguishable from their respective whole rock $^{143}Nd/^{144}Nd$. The isotopic measurements on the melt inclusions are paired with major and trace element concentrations to investigate the mechanisms generating $^{87}Sr/^{86}Sr$ variability in melt inclusions. The lack of significant $^{87}Sr/^{86}Sr$ variability in the Hawaiian melt inclusions (only 251 ppm) from Puu Wahi does not require exotic melt sources or magma mixing models. In contrast, for the Samoan melt inclusions, we present evidence that supports the mixing of isotopically-heterogeneous mantle-derived melts in conjunction with brine interaction as the mechanism generating the observed $^{87}Sr/^{86}Sr$ and trace element variability in the melt inclusions from AVON3-71-2.

Keywords: Melt inclusions, $^{87}Sr/^{86}Sr$, $^{143}Nd/^{144}Nd$, Mantle Geochemistry, TIMS

1. INTRODUCTION

Geochemical studies have dominantly relied on analyses of whole-rock lavas to infer the composition of the mantle beneath ocean island hotspots (e.g., Gast et al., 1964; Hofmann and White, 1982; White, 1985; Zindler and Hart, 1986; Sun and McDonough, 1989; Carlson, 1994; Hofmann, 1997; White, 2010; 2015a; 2015b; Stracke, 2016). However, small blebs of melt trapped in growing magmatic phenocrysts at depth—referred to as melt inclusions—have been shown to host extreme geochemical heterogeneity that is not observed in analyses of individual whole-rock lavas. Melt inclusions from a single lava can host heterogeneous Pb (e.g., Saal et al., 1998, 2005; Yurimoto et al., 2004; Maclennan, 2008; Sakyi et al., 2012; Borisova et al., 2014;

Cabral et al., 2014; Rose-Koga et al., 2012, 2017) and Sr (Jackson and Hart, 2006; Harlou et al., 2009; Sobolev et al., 2011) isotopic compositions that span much of the variability observed in oceanic lavas globally. Despite their volumetrically minor contribution to the whole rock lava, the isotopic diversity preserved in melt inclusions provides important information about mantle melting and the processes that operate in magma chambers. The origin of the chemical and isotopic diversity in melt inclusions remains the source of debate, but has most often been attributed to either assimilation of oceanic crust or mixing of isotopically heterogeneous pristine mantle melts (e.g., Sobolev and Shimizu, 1993; Gurenko and Chaussidon, 1995; Kent et al., 1999; Sobolev et al., 2000; Lassiter et al., 2002; Maclennan et al., 2003a, 2003b; Danyushevsky et al., 2003, 2004; Sobolev et al., 2011).

Only a handful of studies have examined Sr isotopic compositions of olivine hosted melt inclusions from ocean island basalt (OIB) lavas. Jackson and Hart (2006) were the first to target individual olivine-hosted melt inclusions for Sr isotopic analysis, utilizing laser ablation multi-collector inductively coupled plasma mass spectrometry (ICP-MS) to analyze melt inclusions from Samoan picrites. Jackson and Hart (2006) found $^{87}Sr/^{86}Sr$ variability within olivine-hosted melt inclusions from a single basalt as large as 3400 ppm, which is 13% of the total range observed in the lavas from the ocean basins (i.e., 0.7021 [Schilling et al., 1994; Fontignie and Schilling, 1996] to 0.7205 [Jackson et al., 2007]). This result was reinforced by the work of Harlou et al. (2009), who employed micro-milling, traditional column chemistry (to separate Sr), and thermal ionization mass spectrometry (TIMS) to analyze the $^{87}Sr/^{86}Sr$ of individual olivine-hosted melt inclusions. Harlou et al. (2009) found even greater $^{87}Sr/^{86}Sr$ heterogeneity (>6000 ppm) than Jackson and Hart (2006) in olivine-hosted melt inclusions from an Icelandic lava. A more recent laser ablation single-collector ICP-MS study (Sobolev et al., 2011) reported remarkable $^{87}Sr/^{86}Sr$ variability (0.7021 to 0.7081, or ~8500 ppm) in olivine-hosted melt

inclusions from a single olivine-rich scoria (the "Puu Wahi" eruption) from Mauna Loa, Hawaii. These studies collectively appear to demonstrate that intra-basalt Sr isotopic heterogeneity exists within olivine-hosted melt inclusion populations in OIB from several localities, and that whole-rock $^{87}Sr/^{86}Sr$ analyses do not accurately capture the full isotopic variability of the melts that contribute to the geochemical signature of a basalt.

Complementary studies have shown that intra-lava Sr-isotopic variability also exists in other phases in MORB (Bryce and DePaolo, 2004) and OIB. In Samoan lavas significant isotopic disequilibrium has been observed between whole rocks and clinopyroxene separates (as large as ~3100 ppm for $^{87}Sr/^{86}Sr$ and 160 ppm for $^{143}Nd/^{144}Nd$; [Jackson et al., 2009]). More recently Reinhard et al. (2016) observed $^{87}Sr/^{86}Sr$ disequilibrium between aggregated olivines and host whole rocks as large as 1947 ppm (in Samoan lava AVON3-78-1), confirming Jackson and Hart's (2006) observation that melt inclusions hosted in olivines are not always in isotopic equilibrium with the host lava. In summary, there is overwhelming evidence for radiogenic isotopic variability preserved in the various components (clinopyroxene, olivine, melt inclusions) hosted in fresh, young OIB lavas. However, the mechanisms generating the Sr isotopic disequilibrium remain poorly understood. The three studies reporting $^{87}Sr/^{86}Sr$ heterogeneity in melt inclusions (Jackson and Hart, 2006; Harlou et al., 2009; Sobolev et al., 2011) provide no consensus on the mechanisms responsible for the variability.

More recently, Koornneef et al. (2015) utilized high precision isotopic analyses by TIMS in individual olivine hosted melt inclusions from Italian Neogene – Quaternary lavas and found significant $^{87}Sr/^{86}Sr$ and $^{143}Nd/^{144}Nd$ heterogeneity within melt inclusion populations from single lavas. Some of the melt inclusions analyzed by Koornneef et al. (2015) were trapped at sub-crustal depths and the isotopic disequilibrium observed is attributed to mantle heterogeneity. However, in some of the melt inclusions studied the origin of isotopic heterogeneity is uncertain

because the lavas examined were trapped within the continental crust, making it difficult to distinguish between different mechanisms—magma mixing versus continental crust assimilation—that might generate radiogenic isotopic variability in the lavas and the melt inclusions they host (Koornneef et al., 2015).

Analyzing melt inclusions from OIB eliminates the possibility that a magma has assimilated continental crust (but not oceanic crust), which aids in constraining the origin of the isotopic variability in olivine hosted melt inclusions (because oceanic crust is both thinner and less enriched in incompatible trace elements). Here we present the first $^{87}Sr/^{86}Sr$ and $^{143}Nd/^{144}Nd$ measurements by TIMS, paired with major, trace, and volatile-element analyses, from individual olivine hosted melt inclusions erupted at two oceanic hotspots. This study targets olivine-hosted melt inclusions from one Hawaiian scoria (Sobolev et al., 2011) and one from Samoan lava (Jackson and Hart, 2006), both of which were targeted for Sr-isotopic analyses on olivine-hosted melt inclusions by laser ablation ICP-MS in prior studies. We use a different analytical approach—wet chemistry and isotopic analysis by TIMS— (see Koornneef et al., 2015) to obtain precise Sr isotopic data on melt inclusions from the same lavas; an important advantage of the TIMS analytical technique is that it does not suffer from the same uncertainties in correcting for isobaric interferences (e.g. Kr, Rb, Ca dimers) as laser ablation-ICP-MS techniques (Vroon et al., 2008). By pairing the TIMS Sr isotopic data with Nd isotopic analyses and major, trace, and volatile element data on the same melt inclusions, this study provides new constraints on the origin of $^{87}Sr/^{86}Sr$ variability in olivine-hosted melt inclusions in oceanic hotspot lavas.

2. METHODS

2.1. Sample selection

The samples—AVON3-71-2 from Vailulu'u seamount in Samoa (Jackson and Hart, 2006), and an olivine-rich scoria from the Puu Wahi eruption on Mauna Loa, Hawaii (Sobolev et al., 2011) (see Fig. 1)—were chosen for this study based on prior observations of $^{87}Sr/^{86}Sr$ heterogeneity within their olivine-hosted melt inclusion populations. Additionally, each of these samples contain abundant olivines that host large (>100 µm) melt inclusions.

2.1.1. *Vailulu'u sample AVON3*-71-2. This sample is a deeply dredged picrite from Vailulu'u (the active location of the Samoan hotspot) that has been extensively characterized geochemically, including whole-rock major- and trace-element concentrations, $^{87}Sr/^{86}Sr$, $^{143}Nd/^{144}Nd$, $^{208}Pb/^{204}Pb$, $^{207}Pb/^{204}Pb$, $^{206}Pb/^{204}Pb$, $^{176}Hf/^{177}Hf$, and $^{187}Os/^{188}Os$ (Workman et al., 2004; Salters et al., 2011; Jackson and Shirey, 2011). Additionally, major, trace, and volatile-element concentrations were measured in glass (Workman et al., 2006; Kendrick et al., 2015), $^{87}Sr/^{86}Sr$ was measured in individual melt inclusions via laser ablation multi-collector ICP-MS (Jackson and Hart, 2006), $\delta^{18}O$ and $^{3}He/^{4}He$ were reported in olivines (Workman et al., 2004; 2008), $^{87}Sr/^{86}Sr$ and $^{143}Nd/^{144}Nd$ isotopic ratios were measured in clinopyroxene separates (Jackson et al., 2009), and $^{87}Sr/^{86}Sr$ was measured on bulk olivine separates (Reinhard et al., 2016).

2.1.2. Puu Wahi. Puu Wahi is a line of scoria cones on the NE rift zone of Mauna Loa (Lockwood et al., 1995). Olivine-hosted melt inclusions in scoria have the advantage of having been rapidly cooled, resulting in glass melt inclusions. The material sampled is a reticulite scoria hosting abundant euhedral olivines (referred to hereafter as the "Puu Wahi" sample), and material from this flow has been analyzed for major, trace, and select volatile-element (S and Cl) concentrations, $^{87}Sr/^{86}Sr$, $^{207}Pb/^{206}Pb$, and $^{208}Pb/^{206}Pb$ isotopic ratios in olivine-hosted melt inclusions (Sobolev et al., 2011). In the same study, major-element concentrations in the glass matrix and host olivines, trace-element concentrations, and $^{87}Sr/^{86}Sr$ in Puu Wahi matrix glass

were reported. Olivines from Puu Wahi were also used for experimental testing of H diffusion rates in olivine by Gaetani et al. (2012), and a later study measured major element and volatile (H_2O, CO_2, and S) concentrations in olivine-hosted melt inclusions from the Puu Wahi scoria (Wallace et al., 2015).

2.2. Sample Preparation

Sample AVON3-71-2 was crushed using a rock hammer then sieved before olivines were handpicked under a binocular microscope. The Puu Wahi sample is glass rich, and adhering glass had to be removed from the olivines prior to sample preparation. Therefore, the Puu Wahi olivines, but not the AVON3-71-2 olivines, were leached in 2N HF for 10 min at 25°C, then rinsed three times in milli-Q water, then leached in concentrated HNO_3 for 15 min at 25°C, then rinsed again three times in milli-Q water to remove all adhering matrix glass. Olivines that hosted large (>85 µm) melt inclusions were selected from the Samoan (AVON3-71-2, N=10 melt inclusions) and the Hawaiian (Puu Wahi, N=10) lavas. The selected olivines hosting large melt inclusions were inspected under binocular microscope to ensure that there was no remaining matrix glass or basaltic groundmass. Because some olivines host more than one melt inclusion, some of the selected olivines hosting melt inclusions were then cut with a diamond wire saw (150 µm diameter wire) to isolate the largest melt inclusion from each olivine grain; remaining melt inclusions hosted in the same olivine grain hosting the largest melt inclusion were removed by mounting the olivine in Crystalbond™ and grinding the melt inclusions with silicon carbide abrasive paper (See Fig. 2 for graphic of melt inclusion isolation). Most grains required polishing in multiple orientations to remove visible melt inclusions. Through this process, all visible groundmass and/or surface alteration was also removed from the olivines by making strategic cuts with the diamond wire saw and by grinding with silicon carbide (Fig. 2). This method can require 4 to 6 days to isolate a single large melt inclusion from an olivine phenocryst (images of

isolated melt inclusions are shown in Fig. S1). The olivines were then removed from their mounts, sonicated in acetone for 15 min to remove any adhering Crystalbond™, leached in 6N HCl at 25°C for 10 min, and then rinsed three times in milli-Q (i.e., 18.2 MΩ) water.

While the Puu Wahi melt inclusions were dominantly glassy (only 2 melt inclusions required homogenization), all inclusions from AVON3-71-2 were crystalline and necessitated homogenization. Following isolation of melt inclusions by cutting and polishing, olivine fragments hosting a single large melt inclusion were homogenized using a Vernadsky-type heating stage under a microscope at the Laboratoire Magmas et Volcans at the Université Clermont Auvergne in Clermont-Ferrand, France, following the procedure detailed by Le Voyer et al. (2008). Crystalline melt inclusions were bathed in helium during homogenization at 1 atm and the oxygen fugacity was kept between 10^{-10} and 10^{-9} atm. Temperatures of homogenization (where applicable) can be found in Table S1. Samples were quenched after homogenization to avoid recrystallization of the melt inclusions. Samples that burst or cracked during homogenization were discarded and are not considered in this study (note that three melt inclusions from AVON3-71-2 did not fully homogenize, therefore we do not discuss their major or trace element concentrations, but we do present and discuss their Sr and Nd isotopic compositions). The resultant glassy melt inclusions were then exposed by careful grinding and polishing, pressed into an indium mount, re-polished using ¼ µm alumina paste, ultra-sonicated in ethanol (10 minutes) and then distilled water (10 minutes) before major and trace element analysis.

Unlike Harlou et al. (2009), who separated the melt inclusions from the host olivine by micro-drilling, this study does not separate melt inclusions from the olivine. This is because Sr and Nd are highly incompatible in the olivine lattice (Fujimaki et al., 1984; Beattie et al., 1994) and therefore the Sr and Nd budgets of the olivines are dominated by the melt inclusions

(Koornneef et al., 2015). Of course it is not possible to avoid micro-inclusions during sample preparation, but their influence on the Sr (or Nd) isotopic composition of the target melt inclusion will be minimal. For example, the $^{87}Sr/^{86}Sr$ of a 150-micron diameter melt inclusion with $^{87}Sr/^{86}Sr$ of 0.7050 and 300 ppm Sr would be perturbed by only 0.22 ppm if a 5-micron diameter melt inclusion with $^{87}Sr/^{86}Sr$ of 0.7092 (seawater composition) and a Sr concentration of 300 ppm were inadvertently included in the same olivine through sample preparation and digestion.

2.3. Major and Trace Element Analyses

Major-element, Cl and S concentrations of the melt inclusions, and major element concentrations of the olivines, were carried out using the Cameca SX100 electron microprobe hosted at the Laboratoire Magmas et Volcans following the method described by Le Voyer et al. (2008). A focused electron beam with 15kV accelerating voltage and 15nA current was used for analyses of host olivines. For analyses of melt inclusions, an electron beam defocused to 5 µm with 15kV accelerating voltage and 8nA current was used. Analyses of ALV519-4-1 (Melson et al, 2002) and KL2-G (Jochum et al., 2006) were performed throughout the major element analytical session to monitor for instrument drift and data quality, and several standards were analyzed during the Cl and S analytical session (including ALV519-4-1; see Table S2). Reproducibility for basaltic glass reference material ALV519-4-1 was <2% (2 RSD) for SiO_2, Al_2O_3, MgO, and CaO, <3% for TiO_2, ≤5% for FeO and Na_2O, <23% for K_2O, <39% for MnO, and <68% for P_2O_5. Reproducibility is calculated based on repeat analyses of basaltic geologic reference glasses during the same analytical session. Cl and S were measured 5 times consecutively in each melt inclusion and standard using a 40 s cycle, and errors are based on the reproducibility of these consecutive analyses.

Data for melt inclusions, olivines, and geologic reference materials can be found in Tables S1, S2, S3, and S4. Major-element data were corrected for the crystallization of olivine by adding or subtracting equilibrium olivine to the melt inclusions in 0.1% increments until the melt inclusion is in equilibrium with the host olivine. Calculation of equilibrium olivine assumed the olivine-melt K_d of 0.3±0.03 (Roeder and Emslie, 1970; Ford et al., 1983) and assumed that 10% of the total iron in the melt is as Fe^{3+}. These olivine-corrected values are reported in Table S5. Unless stated otherwise, all melt inclusion major (and trace, see below) element compositions discussed in the text have been corrected for olivine fractionation or addition.

Trace element concentrations were measured using a Thermo Scientific Element XR ICP-MS coupled to a Resonetics M-50E 193nm ArF excimer laser housed at Laboratoire Magmas et Volcans. The method followed those outlined in Oulton et al. (2016), with some minor differences as described here. Intensities were normalized to ^{43}Ca as the internal standard. Before all analyses, each spot underwent pre-ablation for 1 s at 10 Hz repetition rate to remove surface contamination. Analyses of melt inclusions and geologic reference materials used a 20 µm spot, and had a repetition rate of 2 Hz with a 50 second dwell time (100 shots per spot); the resulting laser pits were approximately 15 µm deep. The accelerating voltage was scanned between magnet jumps to monitor the peak positions. The following masses were analyzed for the target elements ^{6}Li, ^{7}Li, ^{44}Ca, ^{47}Ti, ^{59}Co, ^{85}Rb, ^{88}Sr, ^{89}Y, ^{90}Zr, ^{93}Nb, ^{137}Ba, ^{139}La, ^{140}Ce, ^{146}Nd, ^{147}Sm, ^{157}Gd, ^{172} Yb, ^{208}Pb, ^{238}U. Analyses were made in low resolution mode using triple mode with a 20% mass window and a 20 ms integration window. NIST612 (Gagnon et al., 2008) and BCR-2 (Jochum et al., 2006) glass were used as standards to generate the calibration curve. Trace element concentrations are shown in Table S3, and olivine-fractionation corrected trace element concentrations of the melt inclusions are shown in Table S6 (for the olivine-fractionation correction, incompatible trace element concentrations were adjusted by the same

proportion as incompatible major elements, e.g., TiO_2). To evaluate the precision and accuracy of analyses, 16 replicate trace-element measurements were performed on a basaltic glass (sample GL07-D52-5 is an incompatible trace element enriched glass from the Easter-Salas y Gomez seamount chain from Kelley et al., 2013) with trace element concentrations similar to those in the Hawaiian melt inclusions from Puu Wahi, but somewhat more depleted than the incompatible trace element enriched Samoan melt inclusions from Vailulu'u. The reproducibility of the trace element concentrations measured in this basaltic glass reference material (see Table S2) was better than 6% (2RSD, n=16), except for Pb (8%) and U and Li (10% and 12%, respectively). The measured concentrations agree with published values from Kelley et al. (2013) to better than 6% for most elements (Ti, Sr, Nb, Ba, La, Ce, Nd, Sm, Yb), and better than 10% for the remaining elements (see Table S2).

2.4. $^{87}Sr/^{86}Sr$ and $^{143}Nd/^{144}Nd$ analysis of melt inclusions by TIMS:

Olivines were plucked from the indium mount and then leached in 15N nitric acid for 2 min at 90°C to remove any adhering indium. Samples were then leached in 1N HCl for 15 min at 25°C to remove any remaining surface contamination and transferred to Teflon beakers. Spikes of ^{84}Sr and ^{150}Nd were added to each the olivine sample, for determination of the total amount of analyte in the sample. The olivines (and the melt inclusions hosted within) were then dissolved in a 4:1 solution of concentrated HF and concentrated HNO_3, and placed on a hot plate at 120°C in capped Teflon beakers for four days. Samples were then dried down and brought up in concentrated HNO_3. Finally, samples were brought up in 200 µl of 3N HNO_3 and loaded on to columns for chemical separation of Sr and Nd. Chemical separation followed the procedures detailed in Koornneef et al. (2015).

The separated Sr was then loaded onto degassed Re filaments for $^{87}Sr/^{86}Sr$ analyses on the Thermo Scientific Triton Plus TIMS housed at the Vrije Universiteit (VU) Amsterdam. Sr

isotopic and abundance measurements were made using ID-TIMS with standard 10^{11} Ω amplifiers and a static multi-collection routine (Koornneef et al., 2015). All $^{87}Sr/^{86}Sr$ ratios were corrected for mass bias relative to an accepted $^{86}Sr/^{88}Sr$ ratio of 0.1194 using an exponential law. Two 200 ng loads of NBS 987 were analyzed during the same analytical session had $^{87}Sr/^{86}Sr$ ratios of 0.710236 (± 0.000009, 2SE) and 0.710243 (± 0.000009, 2SE). All $^{87}Sr/^{86}Sr$ ratios measured on melt inclusions and geologic reference materials are corrected for the offset between the preferred NBS 987 value (0.710240; Thirlwall, 1991) and the average value measured on NBS 987 during the same analytical session. Two aliquots of BHVO-2 (146 and 380 ng of Sr) were processed through all steps of the chemistry, and yielded $^{87}Sr/^{86}Sr$ ratios of 0.703470 (± 0.000010, 2SE) and 0.703458 (± 0.000008, 2SE). Both measured BHVO-2 compositions are within error of the preferred BHVO-2 value of 0.703471 (±0.000020, 2SD), following renormalization to a NBS987 value of 0.710240 (Weis et al., 2006). The average $^{87}Sr/^{86}Sr$ of AGV-1 (loaded to have ~4 ng Sr) run during the same period was 0.704007 (±0.000029 2SD, n=6), which is within error of the preferred AGV-1 value of 0.703981 (±0.000017 2SD; Weis et al., 2006), following renormalization to the preferred NBS987 value of 0.710240.

Neodymium was loaded onto a degassed Re filament for $^{143}Nd/^{144}Nd$ ratio and Nd abundance analyses on the Thermo Scientific Triton Plus using 10^{13} Ω amplifiers in the feedback loop (following procedures from Koornneef et al., 2014 and 2015). The 10^{13} Ω amplifiers yield better signal-to-noise ratios that enhances the precision of isotopic analyses of very small amounts of Nd (Koornneef et al., 2014; 2015). All $^{143}Nd/^{144}Nd$ ratios were corrected for instrumental mass bias to a $^{146}Nd/^{144}Nd$ ratio of 0.7219 using the exponential law. All $^{143}Nd/^{144}Nd$ ratios are corrected for the offset between the measured JNdi value (measured during the same analytical session) and our preferred value (0.512104; Jackson and Carlson

2012). Three 100 ng JNdi standards were run throughout the analytical session using $10^{13}\,\Omega$ amplifiers, and yielded values of 0.512111 (± 0.000032, 2SE), 0.512154 (± 0.000035, 2SE) and 0.512116 (± 0.000035 2SE); the average $^{143}Nd/^{144}Nd$ value was used to correct for the offset of the measured value from the preferred value. Additionally, a 100 pg load of the in-house CIGO standard was run, yielding a $^{143}Nd/^{144}Nd$ value of 0.511357 (± 0.000034, 2SE), which is within error of the long-term average of 100 pg CIGO standard loads run at VU using the same technique (0.511339 ±0.000066 2SD, n=77). Two (9.3 and 23 ng Nd) aliquots of BHVO-2 were processed through all steps of the Nd chemistry with the melt inclusions in this study, and yielded $^{143}Nd/^{144}Nd$ ratios of 0.512969 (± 0.000039, 2SE) and 0.512908 (± 0.000037, 2SE); these values compare well with the Weis et al. (2006) BHVO-2 value of 0.512973 (±0.000011 2SD), following the La Jolla to JNdi conversion from Tanaka et al. (2000) and correcting to a JNdi $^{143}Nd/^{144}Nd$ value of 0.512104. The average $^{143}Nd/^{144}Nd$ of AGV-1 (loaded to have ~200 pg Nd) run during the same period was 0.512787 (±0.000040 2SD, n=4; normalized to a CIGO value of 0.511333), which is within error of the preferred Weis et al. (2006) AGV-1 value of 0.512780 (±0.000013 2SD) following the corrections used above.

Individual Samoan and Hawaiian melt inclusions contained 0.8 to 19.1 ng of Sr (Table 1 & S7) and 0.06 to 1.07 ng of Nd (Table 1 & S8). Total procedural blanks were processed together with the melt inclusions through all steps of column chemistry and mass spectrometry, and were 72 pg for Sr and 6 pg for Nd. Sample-to-blank ratios for Sr analyses varied from 11 to 265, and from 10 to 178 for Nd (see Tables S7 & S8). A sample-to-blank threshold was applied to ensure that samples where blank provided a significant contribution to the uncertainty were not considered, and the following thresholds are employed to reduce uncertainty associated with the blank correction (see Fig. S2): Only analyses with Sr sample/blank ratios greater than 25, and Nd sample/blank ratios greater than 40, are considered in Sections 3 (Data and Observations) and

Section 4 (Discussion). Nonetheless, all Sr and Nd isotopic data, including melt inclusions that have unacceptably low sample/blank ratios, are reported in Tables S7 and S8. Blank corrections were made using the laboratory blank $^{87}Sr/^{86}Sr$ and $^{143}Nd/^{144}Nd$ ratios previously determined for the Sr and Nd chemistry at VU (Koorneef et al., 2015; Knaf et al., 2017); the total procedural blank isotopic ratio used for correction is 0.711120 ± 0.000050 (n =3) for $^{87}Sr/^{86}Sr$ and 0.511856 ± 0.000090 (n = 3) for $^{143}Nd/^{144}Nd$.

3. DATA AND OBSERVATIONS

Major elements for the melt inclusions analyzed in this study are presented in Fig. 3 (and Table S1 & S5). Like all Mauna Loa lavas, the 10 olivine-hosted melt inclusions analyzed in this study are tholeiitic, whereas three melt inclusions from AVON3-71-2 are alkalic and four are transitional (Fig. 3). The MgO contents of the Puu Wahi (11.8-14.1 wt %; Table S5) and AVON3-71-2 (10.9-16.3 wt %; Table S5) melt inclusions fall within the range identified in previously analyzed Mauna Loa and Vailulu'u lavas, respectively (Fig. 3). With the exception of one Puu Wahi and one AVON3-71-2 melt inclusion, the melt inclusions from both samples have significantly lower FeO concentrations than previously analyzed Mauna Loa and Vailulu'u whole rocks (Fig. 3). The apparent depletion in Fe in most of the melt inclusions, due to re-equilibration between the melt inclusion and the host olivine, is similar to previous observations of "Fe-loss" from olivine-hosted melt inclusions at other localities (Danyushevsky et al., 1992, 2000; Sobolev and Danyushevsky, 1994; Gaetani and Watson, 2000; Kent, 2008).

Following correction for olivine fractionation or addition to be in equilibrium with the host olivine, the primitive mantle (McDonough and Sun, 1995) normalized incompatible trace element patterns of the melt inclusions from AVON3-71-2 are similar to that of the host whole rock (Fig. 4). The AVON3-71-2 melt inclusions have no clear Sr anomalies relative to elements

of similar compatibility. (Sr anomalies are represented by $Sr/Sr^* = Sr_N/(Nd_N*Sm_N)^{0.5}$, where N represents normalization to primitive mantle [McDonough and Sun, 1995]). In the Puu Wahi melt inclusions, trace element concentrations of the most incompatible elements are similar to their host glass. In contrast, the less incompatible elements (Zr, Sm, Ti, Gd, Y, Tb) tend to have lower concentrations in the melt inclusions relative to host glass analyzed by Sobolev et al. (2011), but we do not have an explanation for this observation. The Puu Wahi melt inclusions show positive Sr anomalies (average Sr/Sr* = 1.37) that are generally larger in magnitude than the host glass (Sr/Sr*= 1.14; Fig. 4).

Figure 5a presents previously-published $^{87}Sr/^{86}Sr$ data obtained on various components of the Samoan lava AVON3-71-2 for comparison with the new $^{87}Sr/^{86}Sr$ reported on melt inclusions here, and include bulk whole rock $^{87}Sr/^{86}Sr$ (0.705943; Workman et al., 2004), laser ablation multi-collector ICP-MS data from melt inclusions (which were previously found to vary from 0.70459 to 0.70602; Jackson and Hart, 2006), bulk clinopyroxene separates (divided into two sub-populations based upon color: green [0.705485] and black [0.705545]; Jackson et al., 2009), and aggregated olivine separates (also sub-divided based upon olivine color: green [0.705404] and brown [0.705436]; Reinhard et al., 2016). The new $^{87}Sr/^{86}Sr$ data on individual olivine-hosted melt inclusions analyzed by TIMS in this study have $^{87}Sr/^{86}Sr$ values that range from 0.705193-0.705853 (936 ppm variability), which represents 44% of the total variability observed in previously analyzed whole rocks from Vailulu'u seamount. The $^{87}Sr/^{86}Sr$ measured in AVON3-71-2 melt inclusions in this study are consistent with previously observed values obtained on a separate suite of melt inclusions analyzed by Jackson and Hart (2006) using laser ablation multi-collector ICP-MS, but the new data (0.705193- 0.705853; n=6) span only 46% of the range of $^{87}Sr/^{86}Sr$ values identified in the laser ablation multi-collector ICP-MS data (0.70459 to 0.70602; n=12). All melt inclusions from AVON3-71-2 in this study (by TIMS) and in a prior

study (by laser ablation multi-collector ICP-MS), as well as all clinopyroxene separates and bulk aggregate olivines from this lava, have $^{87}Sr/^{86}Sr$ that is similar to or lower than the whole-rock (0.705943; Workman et al., 2004).

All published $^{87}Sr/^{86}Sr$ data from the Puu Wahi flow is presented in Fig. 5b, including data on the host glass (this study), $^{87}Sr/^{86}Sr$ on melt inclusions from 137 melt inclusions by laser ablation single-collector ICP-MS (Sobolev et al., 2011), and new $^{87}Sr/^{86}Sr$ data in melt inclusions by TIMS reported here. Sobolev et al. (2011) found extreme $^{87}Sr/^{86}Sr$ variability (~8500 ppm) in a suite of melt inclusions from Puu Wahi (0.7021–0.7081; n=137). In contrast, the Puu Wahi melt inclusions analyzed in this study show only 251 ppm of total variability (0.703761–0.703938, n=9), which is nearly 34 times less variability than observed by Sobolev et al. (2011). Additionally, the Puu Wahi melt inclusions analyzed in this study have $^{87}Sr/^{86}Sr$ ratios that are less than, or within error of, the $^{87}Sr/^{86}Sr$ of the matrix glass (0.703912 ±0.000008, 2SE; this study) hosting the olivines. This stands in contrast to the Puu Wahi melt inclusions analyzed by Sobolev et al. (2011), which have $^{87}Sr/^{86}Sr$ ratios that are higher (64 melt inclusions) and lower (73 melt inclusions) than the matrix glass.

Figure 6 presents the $^{143}Nd/^{144}Nd$ and $^{87}Sr/^{86}Sr$ data of the Samoan and Hawaiian melt inclusions analyzed in this study (see Table 1). The three Vailulu'u sample AVON3-71-2 melt inclusions with Nd-isotopic data have $^{143}Nd/^{144}Nd$ ratios of 0.512705 (±0.000052, 2SE) to 0.512809 (±0.000065, 2SE), and are thus within error of previously reported whole rock $^{143}Nd/^{144}Nd$ measurements from Vailulu'u (Workman et al., 2004). Similarly, the three Puu Wahi melt inclusions with $^{143}Nd/^{144}Nd$ data have ratios that are within error of one another (from 0.512800 ± 0.000050 to 0.512900 ± 0.000064) and within error of previously published $^{143}Nd/^{144}Nd$ from Mauna Loa whole rocks. Notably, Fig. 6 shows that the internal errors obtained on individual melt inclusions from Samoa AVON3-71-2 (the 2σ standard errors range from 102

to 152 ppm, n=3) and Puu Wahi (91 to 126 ppm, n=3) are similar to the errors obtained using an older generation TIMS instrument on $^{143}Nd/^{144}Nd$ analyses of MORB and OIB whole rocks by DePaolo and Wasserburg (1976) (60 to 90 ppm, n=3). Nonetheless, the precision (91 to 152 ppm, 2RSE) on $^{143}Nd/^{144}Nd$ analyses of individual melt inclusions is insufficient to resolve any intra-lava heterogeneity in this sample suite.

The Cl/Nb ratios vary from 13.4 to 16.6 in AVON3-71-2 melt inclusions, with the exception of melt inclusion AVON3-71-2-8 (33.6) (Fig. 7; Table S6). Similarly, high Cl/Nb ratios (up to 33.0 see Fig. 7) were observed in pillow rim glasses dredged from the flanks of Vailulu'u (Workman et al., 2006; Kendrick et al., 2015). The Puu Wahi melt inclusions have Cl/Nb ratios (4.5–10.1) that are within the range suggested for pristine mantle melts (Cl/Nb < 11; Rose-Koga et al., 2012). Cl/Nb (and Cl/K) do not co-vary with $^{87}Sr/^{86}Sr$ in the Puu Wahi or AVON3-71-2 melt inclusions analyzed in this study (Fig. 7).

However, $^{87}Sr/^{86}Sr$ ratios show a positive relationship with Rb/Sr and Ba/Nb ratios in AVON3-71-2 melt inclusions. The melt inclusions from AVON3-71-2 have Ba/Nb ratios that vary from 5.5 to 6.2, falling within the range of Ba/Nb previously reported on whole rock lavas from Vailulu'u (Fig. 8). The AVON3-71-2 melt inclusions have a smaller range in Rb/Sr (0.060–0.085) than previously observed in Vailulu'u lavas (0.051–0.081; Workman et al., 2004) (Fig. 9), but they fall within the range of Rb/Sr ratios (0.047–0.103) reported by Jackson and Hart (2006) in melt inclusions from the same sample (AVON3-71-2).

The Puu Wahi melt inclusions have a broad range of Ba/Nb ratios (8.6–12.0) that fall within the variability observed in Mauna Loa lavas (Jackson et al., 2012; see Fig. 8). However, Sobolev et al. (2011) reported greater variability in Puu Wahi melt inclusions (Ba/Nb ratios of 7.7–15.4) than we report in melt inclusions from the same lava. Similarly, Rb/Sr ratios in the Puu Wahi melt inclusions analyzed in this study (0.019–0.023; Fig. 9) exhibit an order of magnitude

less variability than the Rb/Sr ratios observed in melt inclusions analyzed (0.004–0.045) by Sobolev et al. (2011). Finally, Sr isotopes in melt inclusions do not correlate with Rb/Sr in the new Puu Wahi melt inclusion dataset or in the dataset of Sobolev et al. (2011). However, in the Puu Wahi melt inclusions from this study there is a positive relationship between $^{87}Sr/^{86}Sr$ and Ba/Nb (Fig. 8), but no equivalent correlation is present in the Sobolev et al. (2011) dataset.

4. DISCUSSION. Exploring mechanisms for generating $^{87}Sr/^{86}Sr$ variability in melt inclusions.

Significant $^{87}Sr/^{86}Sr$ heterogeneity has been shown to exist between olivine-hosted melt inclusions within a single lava (Jackson and Hart, 2006; Harlou et al., 2009; Sobolev et al., 2011; Koornneef et al., 2015; this study). However, the mechanism by which $^{87}Sr/^{86}Sr$ heterogeneity in melt inclusions is generated remains poorly understood. The observation that olivines in a single lava can host melts with variable $^{87}Sr/^{86}Sr$ necessitates that melts with variable $^{87}Sr/^{86}Sr$ were present when olivine crystallized in the magma system, and that olivines captured these heterogeneous melts as melt inclusions. Below, we discuss potential mechanisms for generating the heterogeneous melts trapped in the AVON3-71-2 and Puu Wahi melt inclusions: 1) mixing of mantle-derived melts with variable $^{87}Sr/^{86}Sr$, and 2.) interaction with brines, in the supplementary material we discuss 3.) assimilation of altered oceanic crust (AOC), and 4.) assimilation of unaltered gabbro in the deep oceanic crust. After acquiring heterogeneous $^{87}Sr/^{86}Sr$ and becoming entrapped in olivine, the olivine-hosted melt inclusion populations are assembled within magmatic plumbing systems and erupted.

Previous studies (Koornneef et al., 2015; Reinhard et al., 2016) argue that olivines encapsulate melts and preserve their $^{87}Sr/^{86}Sr$ ratios due to the incompatibility of Sr in olivine (Beattie, 1994) and slow Sr diffusion rates through olivine (Remmert et al., 2008). Additionally,

both samples have relatively low Rb/Sr ratios (see Data and Observations section) and are visually fresh and young—Puu Wahi erupted at 910 yr B.P. (Lockwood et al., 1995) and AVON3-71-2 is <8 ka (Sims et al., 2008)—such that the radiogenic decay of ^{87}Rb to ^{87}Sr (half life of ~49 Ga) has not significantly modified the ^{87}Sr/^{86}Sr of these melt inclusions post entrapment. Therefore, we assume all ^{87}Sr/^{86}Sr heterogeneity in the melt inclusions examined here is the result of pre-entrapment processes. In the following sections we evaluate potential mechanisms that contribute to heterogenous ^{87}Sr/^{86}Sr in melt inclusions: new data from Vailulu'u melt inclusions are explored, followed by a discussion of the isotopically homogeneous Puu Wahi melt inclusions.

*4.1. Vailulu'u (*Samoan sample AVON3-71-2)

4.1.1. Mixing of mantle-derived melts with heterogenous ^{87}Sr/^{86}Sr.

The mixing of pristine mantle melts with heterogeneous ^{87}Sr/^{86}Sr has been proposed as a mechanism for generating the highly heterogeneous ^{87}Sr/^{86}Sr ratios in olivine-hosted melt inclusions, including melt inclusions from AVON3-71-2 (Jackson and Hart, 2006). If pristine mantle melts have heterogenous ^{87}Sr/^{86}Sr ratios that reflect their source, then the mixing of these melts as olivine is crystallizing (and trapping melt inclusions) could generate the observed ^{87}Sr/^{86}Sr and trace element ratio heterogeneity in the AVON3-71-2 melt inclusions.

A simple binary mixing model can be used to generate the heterogeneity observed in the AVON3-71-2 melt inclusions using known whole-rock lava compositions from the Samoan hotspot as hypothetical mixing endmembers. In the model, the geochemically enriched endmember is mixed with a geochemically depleted endmember, we identify two endmembers that are suited for generating the trends exhibited by the melt inclusions (see description of endmembers in Fig. 8 caption). A mixture of these two endmembers generates trends that fit the

observed relationships between $^{87}Sr/^{86}Sr$ and incompatible trace element ratios (e.g. Rb/Sr and Ba/Nb). The observed correlation between trace element ratios (Rb/Sr and Ba/Nb) and $^{87}Sr/^{86}Sr$, together with the observation that the AVON3-71-2 melt inclusions fall along the model mixing line, support the hypothesis that the mixing of mantle-derived melts with heterogeneous $^{87}Sr/^{86}Sr$ prior to eruption could generate the observed $^{87}Sr/^{86}Sr$ variability.

4.1.2. Assimilation.

While the mixing of heterogenous mantle melts could generate the observed $^{87}Sr/^{86}Sr$ heterogeneity and the concomitant incompatible trace element ratio (Rb/Sr and Ba/Nb) variability, magma mixing alone cannot explain the enrichments in Cl found in the AVON3-71-2 melt inclusions (Fig. 7). The elevated Cl/Nb ratios in the AVON3-71-2 melt inclusions range up to values (33.6) that are above the range for pristine mantle-derived melts, suggesting that assimilation of seawater derived materials has modified the Cl concentrations the AVON3-71-2 melt inclusions. However, it is important to evaluate whether the $^{87}Sr/^{86}Sr$ was modified by this mechanism.

The assimilation of seawater-derived materials—including AOC, seawater, and brines—can modify the $^{87}Sr/^{86}Sr$ of a melt. This is because seawater-derived materials can host elevated concentrations of Sr and inherit an $^{87}Sr/^{86}Sr$ ratio from seawater (which contains ~7.85 ppm Sr [Bernat et al., 1972] with radiogenic $^{87}Sr/^{86}Sr$ [0.709179; Mokadem et al., 2015]). If olivine crystallizes during or after magmatic assimilation of seawater-derived materials, the melt inclusions would trap signatures of this assimilant.

Several studies have suggested that melt inclusions may be more sensitive recorders of the assimilation of seawater derived materials than whole rock lavas because 1.) crystallization of olivine is enhanced at the magma chamber margins due to cooler temperatures near the

magma chamber walls and 2.) melts trapped by growing olivine at magma chamber margins are more likely to have interacted with the wall rock than melts closer to the interior of the chamber (Kamenetsky et al., 1998; Bédard et al., 2000; Danyushevsky et al., 2003, 2004). If assimilation is generating $^{87}Sr/^{86}Sr$ heterogeneity, and if melts hosting signatures of assimilation are preferentially trapped in growing magmatic phenocrysts near magma chamber walls, then extreme $^{87}Sr/^{86}Sr$ compositions will be recorded disproportionately in olivine-hosted melt inclusions relative to the bulk lava. This conceptual model may explain the high degree of $^{87}Sr/^{86}Sr$ variability observed in melt inclusions from some lavas.

Identifying signatures of assimilated seawater-derived materials can be difficult due to the geochemical variability in these materials. While the $^{87}Sr/^{86}Sr$ of modern seawater is homogeneous, with a value of 0.709179 (Mokadem et al., 2015), oceanic crust and alteration products can have $^{87}Sr/^{86}Sr$ ratios that range from ~0.7021 in fresh MORB (Schilling et al., 1994; Fontignie and Schilling, 1996) to as high as 0.7257 (Hauff et al., 2003) in highly altered components within early Mesozoic Pacific oceanic crust (where enrichment of Rb in AOC [e.g., Kelley et al., 2003] results in high Rb/Sr that generates high time-integrated $^{87}Sr/^{86}Sr$ via ^{87}Rb decay).

Chlorine provides a powerful tool for identifying assimilation of seawater-derived materials in oceanic lavas because it is fluid mobile and not efficiently subducted into the mantle. Thus, recycled materials in hotspot lavas are not expected to have high Cl/K (e.g., Kendrick et al., 2013) or Cl/Nb (Rowe and Lassiter, 2009), and mantle-derived lavas that have not assimilated seawater-derived materials have low Cl/Nb ratios (e.g. 5-17; Rowe et al., 2015; Michael and Cornell, 1998; Saal et al., 2002; Stroncik and Haase, 2004; Rowe and Lassiter, 2009).

In contrast, seawater and seawater-derived materials (including brines and altered oceanic crust) are rich in Cl (e.g., Sano et al., 2008; Kendrick et al., 2013; 2015; Van den Bleeken and Koga, 2015). Due to alteration by seawater, altered oceanic crust becomes enriched in Cl and other diagnostic elements (including Li, B, K, Rb, Cs, and U; e.g., Kelley et al., 2003; Staudigel, 2003; Sano et al., 2008). However, seawater and brines are poor in Nb relative to mantle-derived melts. As a result, altered oceanic crust inherits high Cl/Nb ratios (and high Cl/K, implied hereafter; Jambon et al., 1993; Michael and Cornell, 1998; Kent et al., 1999a, 1999b, 2002; Lassiter et al., 2002; Kendrick et al., 2013, 2015) relative to pristine mantle-derived melts. Therefore, assimilation of altered oceanic crust by magmas transiting through oceanic crust can elevate the magmatic Cl concentrations relative to similarly incompatible elements, like Nb, resulting in high Cl/Nb ratios in lavas (and melt inclusions) erupted at the surface (e.g., Michael and Cornell, 1998; Kent 1999a, 1999b; Kendrick et al., 2013, 2015).

When used in tandem, Cl concentrations and $^{87}Sr/^{86}Sr$ present a powerful tool for evaluating the presence of assimilated seawater derived materials in lavas. Altered oceanic crust has elevated Cl (and Cl/Nb) and higher $^{87}Sr/^{86}Sr$ relative to fresh MORB (Staudigel et al., 1995, 1996; Bach et al., 2003; Hauff et al., 2003; Staudigel, 2003). Thus, if assimilation of seawater derived materials is the mechanism responsible for generating the observed $^{87}Sr/^{86}Sr$ variability in olivine-hosted melt inclusions, then $^{87}Sr/^{86}Sr$ should correlate with indicators of assimilated seawater derived materials (e.g, Cl/Nb). However, Cl and Cl/Nb do not covary with $^{87}Sr/^{86}Sr$ (Fig. 7). This requires that the melt assimilated material that modifies the Cl (and Cl/Nb) of the melt inclusions but does not significantly modify $^{87}Sr/^{86}Sr$. Assimilation of deep crustal gabbros and altered oceanic crust are unlikely candidates (see Supplementary Text). However, as we explain below, a brine interaction model may be consistent with the observations of this study.

Interaction with brines. Kendrick et al. (2015) analyzed Samoan glasses for F, Cl, Br, and I concentrations and reported a Cl/Nb ratio of 32.6 in pillow rim glass from the same lava that we examine here (AVON3-71-2), similar to the Cl/Nb ratio we measured in melt inclusion AVON3-71-2-8 (33.6). Together with evidence from Br and I data, Kendrick et al. (2015) attribute 75% of the Cl in the AVON3-71-2 glass to the interaction with brines (totaling 0.45 wt.% of the mixture, assuming the brines are composed of 55±15 wt% salts). Other glasses from Vailulu'u (as well as submarine glasses from several other Samoan volcanoes, Ta'u, Malumalu, Muli and Taumatau) also exhibit evidence for significant contribution of Cl from brine (Kendrick et al., 2015). Similar to our results on melt inclusions from AVON3-71-2, Kendrick et al. (2015) and Workman et al. (2006) did not observe a correlation between indicators of assimilation and $^{87}Sr/^{86}Sr$ in the Samoan glasses they analyzed. Kendrick et al. (2013; 2015) suggest that the brine the Samoan melts interacted with had low Sr concentrations and therefore interaction with brines could generate the observed Cl enrichment (and high Cl/Nb ratios) without significantly modifying the $^{87}Sr/^{86}Sr$ of the melt.

Extrapolating from the results on Samoan submarine pillow glasses (including the pillow glass from AVON3-71-2) of Kendrick et al. (2015), the data presented here on AVON3-71-2 melt inclusions are consistent with brine interaction prior to entrapment if the brine is Sr poor (as suggested by Kendrick et al., 2015). For example, melt inclusion AVON3-71-2-8 has a Cl/Nb ratio of 33.6, which is indicative of a significant enrichment in Cl, and has a similar Cl/Nb to the AVON3-71-2 pillow rim glass (32.6) which was attributed to interaction with brine (where the expected Cl/Nb for pristine Vailulu'u glasses unmodified by brine is ≤10; e.g., Kendrick et al., 2015). Further, the interaction with brines may explain why some AVON3-71-2 melt inclusions have elevated Cl/Nb, yet there is no observed correlation between $^{87}Sr/^{86}Sr$ and Cl/Nb in the melt inclusion suite from this lava.

The influence of interaction with brines on the AVON3-71-2 melt inclusions can be tested using a simple mixing model. We adopt a 55% salt brine (~30 wt.% of the brine is Cl) composition (from Kendrick et al., 2015) that has $^{87}Sr/^{86}Sr$ of seawater (0.709179; Mokadem et al., 2015), a Sr concentration of Mid-Atlantic Ridge hydrothermal fluids (11.1 ppm; Schmidt et al., 2007), and a Nb concentration of 0.2 ppb (le Roux et al., 2006). The brine is mixed into a melt with a Cl/Nb ratio equal to the lowest Cl/Nb Vailulu'u glass (sample AVON3-72-2: Cl = 670 ppm, Nb = 67 ppm Cl/Nb = 10.0; Workman et al., 2006) and $^{87}Sr/^{86}Sr$ equal to the lowest $^{87}Sr/^{86}Sr$ inclusion from this study (AVON3-71-2-9)(Fig. 7). In our model, a mixture with only 0.52% brine would generate the maximum Cl/Nb (33.6) of the AVON3-71-2 melt inclusions reported here (Fig. 7). This value is similar in magnitude to the 0.45% brine interaction for the AVON3-71-2 pillow glass from Kendrick et al. (2015). The assimilation of such a small amount of brine increases the $^{87}Sr/^{86}Sr$ ratio of the melt by only 0.5 ppm, more than an order of magnitude less than the uncertainty on the $^{87}Sr/^{86}Sr$ analyses by TIMS reported here. Therefore, interaction with brine can generate elevated Cl/Nb in Vailulu'u melts without significantly modifying the $^{87}Sr/^{86}Sr$ of the melt. The lack of correlation between Cl/Nb and $^{87}Sr/^{86}Sr$ in AVON3-71-2 melt inclusions, which host a wide range of Cl/Nb (13.4 to 33.6), is explained by brine interaction withmelts prior to entrapment in growing olivines.

Based on the magma mixing model described in section 4.1.1., binary mixing of geochemically-enriched and geochemically-depleted magmas can generate relationships between $^{87}Sr/^{86}Sr$ and Rb/Sr and Ba/Nb and, critically, none of these ratios are significantly impacted by interaction with brines owing to low Sr, Nb, Rb (Schmidt et al., 2007), and Ba (Charlou et al., 2002) content of the brines relative to the alkalic Samoan melts. However, elevated Cl/Nb ratios in the suite of AVON3-71-2 melt inclusions indicate that either (or both) of the endmember magmas in the magma mixing model (Section 4.1.1) interacted with a small amount of brine,

variably influencing the melt inclusion Cl budgets (and Cl/Nb ratios) prior to entrapment. Unfortunately, given the existing suite of data, it is not possible to evaluate whether magma mixing or brine interaction occurred first, but the data do suggest that both processes operated on the melt trapped in the AVON3-71-2 melt inclusions.

4.2. Puu Wahi (Mauna Loa, Hawaii)

4.2.1. $^{87}Sr/^{86}Sr$ heterogeneity in melt inclusions from Puu Wahi

The Puu Wahi melt inclusions analyzed in this study demonstrate limited $^{87}Sr/^{86}Sr$ variability (only 251 ppm, 0.703761– 0.703938, n=9). However, this limited variability is still greater than the reproducibility of $^{87}Sr/^{86}Sr$ measurements on similarly sized aliquots of Sr (±43 ppm 2RSD, based on replicate analyses of 4 ng Sr loads of AGV-1; see Methods), suggesting a very limited range of true Sr-isotopic variability in the suite of Puu Wahi melt inclusions examined here. Given the relatively narrow range of $^{87}Sr/^{86}Sr$ ratios, it is difficult to evaluate the mechanisms responsible for generating the $^{87}Sr/^{86}Sr$ variability observed in the Puu Wahi melt inclusions analyzed in this study.

The Puu Wahi melt inclusions analyzed in this study do not show a correlation between $^{87}Sr/^{86}Sr$ and Cl/Nb (Fig. 7), and they all have low Cl/Nb ratios (<10.1), so it is unlikely that assimilation of seawater derived materials is responsible for the limited $^{87}Sr/^{86}Sr$ variability observed the Puu Wahi melt inclusions (Lassiter et al., 2002; Workman et al., 2006; Kendrick et al., 2014; Cabral et al., 2014). Additionally, these Puu Wahi melt inclusions have Sr/Sr*>1.2, but there is no relationship between $^{87}Sr/^{86}Sr$ and Sr/Sr* (Fig. S5), which argues against the assimilation of deep oceanic gabbro as the sole mechanism generating the limited $^{87}Sr/^{86}Sr$ heterogeneity (e.g., Saal et al., 2007). Finally, the Puu Wahi melt inclusions show no relationship

between $^{87}Sr/^{86}Sr$ and Rb/Sr, which excludes simple two-component mixing of magmas as the sole mechanism generating $^{87}Sr/^{86}Sr$ variability in these melt inclusions.

In contrast to the narrow range of $^{87}Sr/^{86}Sr$ ratios obtained on Puu Wahi melt inclusions from this study, Sobolev et al. (2011) identified much greater variability (nearly 34 times greater) in their suite of Puu Wahi olivine-hosted melt inclusions (~8500 ppm of $^{87}Sr/^{86}Sr$ varibility, 0.7021–0.7081; n=137). The extreme isotopic variability observed by Sobolev et al. (2011) raises some key questions: Why does their dataset exhibit a significantly greater range in $^{87}Sr/^{86}Sr$ in Puu Wahi melt inclusions than the dataset generated in this study, and how can we reconcile their results with the relatively narrow range in $^{87}Sr/^{86}Sr$ observed in the melt inclusions in this study?

One possible explanation is that our sample size (n= 9) is significantly smaller than Sobolev et al.'s (2011) (n = 137), and the more limited $^{87}Sr/^{86}Sr$ heterogeneity observed in this study (251 ppm) compared to the Sobolev et al. (2011) study (~8500 ppm) is the result of the small sample size. However the observed trace element heterogeneity (e.g. Ba/Nb; Fig. 8) is similar in magnitude to that observed by Sobolev et al. (2011) suggesting that we did not analyze an anomalously homogenous suite of Puu Wahi melt inclusions. A second possible reason for the contrast between the results of this study and those of Sobolev et al. (2011) is the relative uncertainties of analyses reported; the reproducibility of the $^{87}Sr/^{86}Sr$ ratio during repeat $^{87}Sr/^{86}Sr$ analyses of individual Puu Wahi melt inclusions by Sobolev et al. (2011) vary significantly, but average errors are ±1660 ppm (2RSE),and are as high as ±4376 ppm (2 RSE, melt inclusion 1441A). This error is similar to the total range observed in the Puu Wahi melt inclusions suite (~8500 ppm) observed by Sobolev et al. (2011). By comparison, the Puu Wahi melt inclusions examine here have errors ranging from only ±14 to ±56 ppm (2 RSE) (and repeat $^{87}Sr/^{86}Sr$ analyses of AGV-1—loaded to have ~4 ng—using the TIMS technique in this study reproduced

to within ± 41 ppm (2 RSD, N=6)). Looking ahead, it will be important to prospect for highly heterogeneous $^{87}Sr/^{86}Sr$ melt inclusions--like those observed in Sobolev et al.'s (2011) study--in a larger suite of Puu Wahi melt inclusions using the TIMS technique employed here.

4.5. Conclusions

In this study, we present the first paired $^{87}Sr/^{86}Sr$ and $^{143}Nd/^{144}Nd$ data on individual olivine-hosted melt inclusions from OIB lavas from Hawaii (sample from the Puu Wahi eruption of Mauna Loa) and Samoa (from Vailulu'u volcano). The combination of isotopic and trace-element analyses on individual olivine-hosted melt inclusions allows for the identification of processes that can modify mantle melts prior to eruption. In the suite of melt inclusions from the Samoa AVON3-71-2 lava, we report 936 ppm variability in $^{87}Sr/^{86}Sr$ in six melt inclusions, and these new data (obtained using a TIMS technique) exhibit 46% of the variability in $^{87}Sr/^{86}Sr$ reported on a suite of 12 melt inclusions from this lava analyzed by laser ablation multi-collector ICP-MS (Jackson and Hart, 2006). For the Samoan melt inclusions, we show that the mixing of isotopically heterogenous mantle-derived melts may be an important mechanism generating the observed $^{87}Sr/^{86}Sr$ heterogeneity, and that localized interaction with small amounts (<1%) of brine generates the observed Cl enrichments and high Cl/Nb ratios (up to 33.6). The relatively homogeneous $^{87}Sr/^{86}Sr$ we report in Puu Wahi melt by TIMS (251 ppm variability in $^{87}Sr/^{86}Sr$ on nine melt inclusions) identified here contrasts with previously reported extreme $^{87}Sr/^{86}Sr$ variability (~8500 ppm variability in $^{87}Sr/^{86}Sr$ on 137 melt inclusions) in melt inclusions from the same eruption using a laser ablation single-collector ICP-MS technique. We were able to show that heterogeneous $^{87}Sr/^{86}Sr$ in Samoan melt inclusions using measured using LA-MC-ICP-MS are can be replicated using a TIMS technique (this study and Reinhard et al., 2016). Therefore, it will be important to employ a TIMS technique to confirm the highly heterogeneous (and

extremely radiogenic) $^{87}Sr/^{86}Sr$ compositions identified in Puu Wahi melt inclusions by Sobolev et al. (2011), but on a larger suite of melt inclusions than was analyzed in this study.

Figures

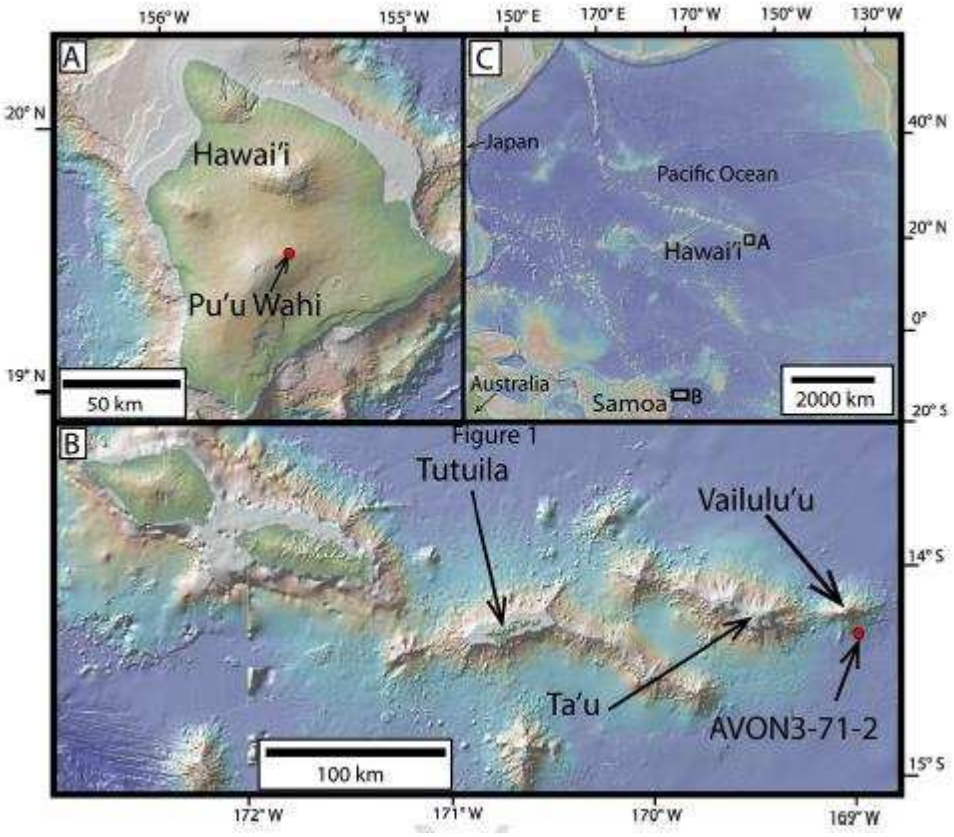

Figure 1

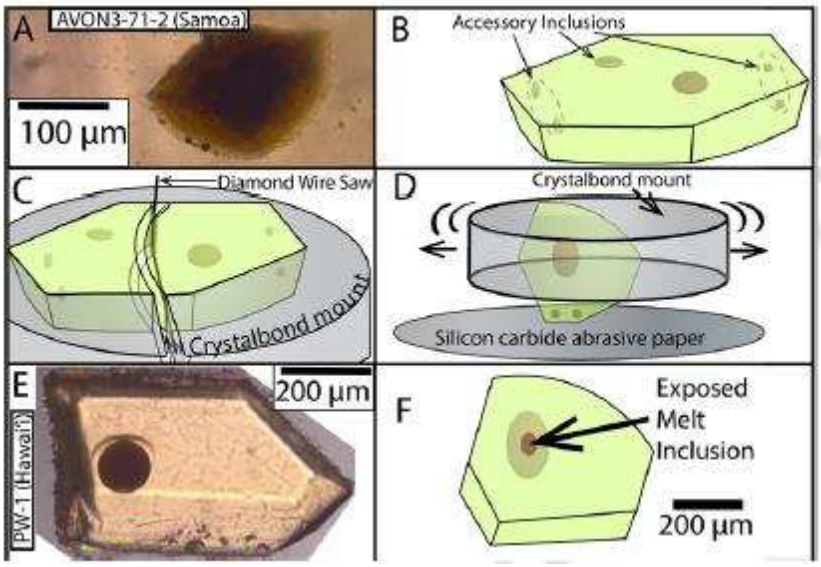

Figure 2

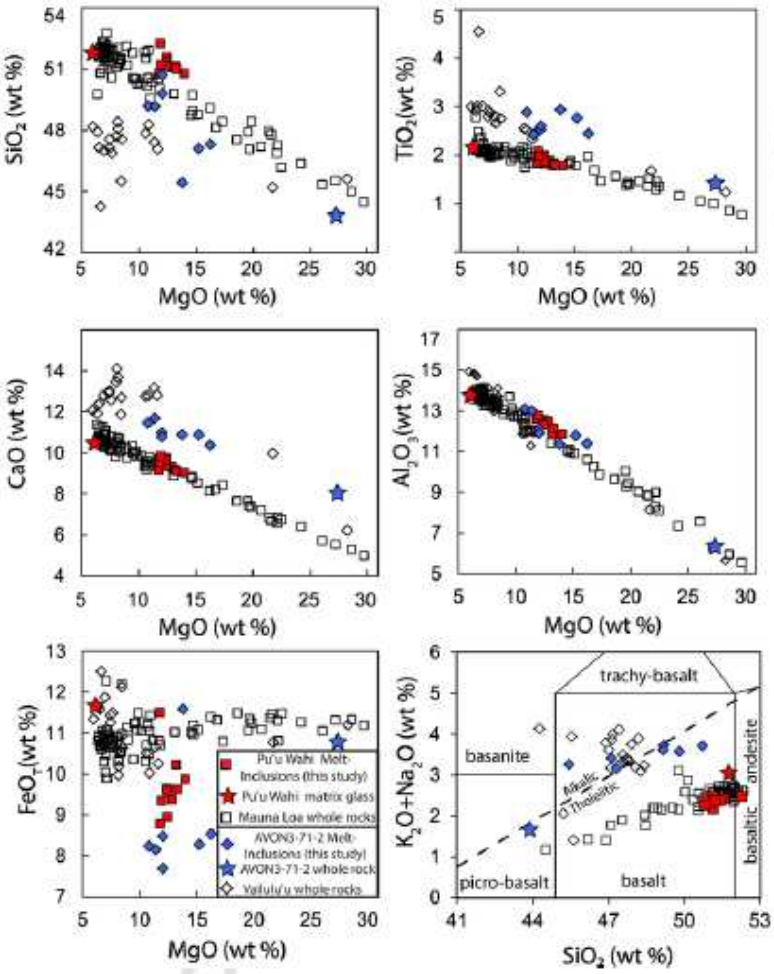

Figure 3

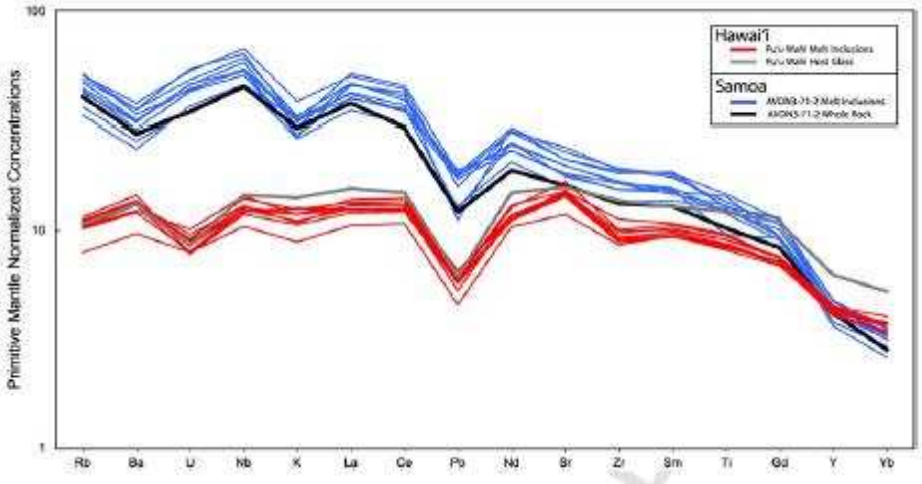

Figure 4

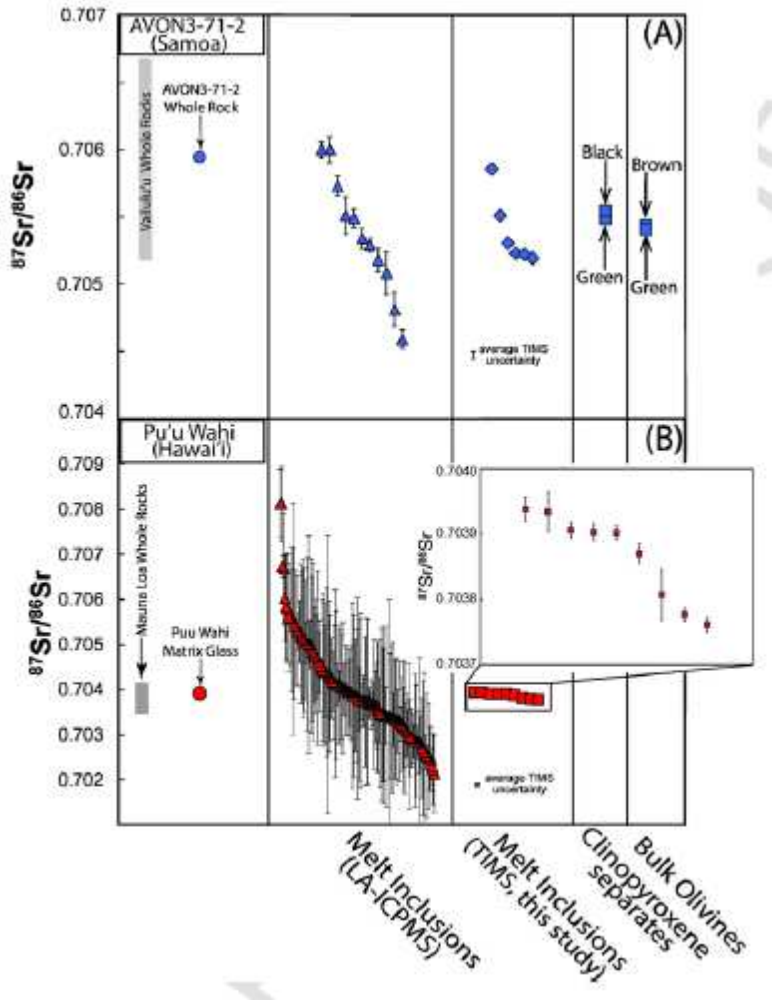

Figure 5

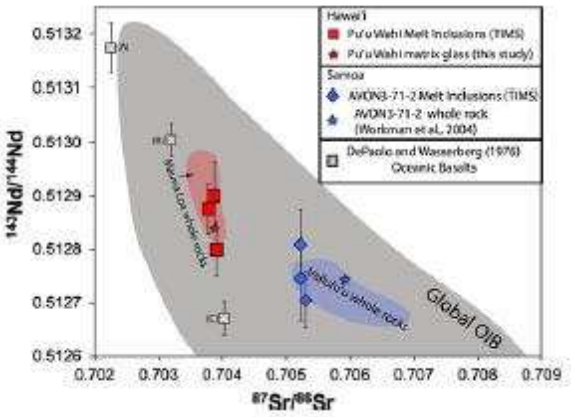

Figure 6

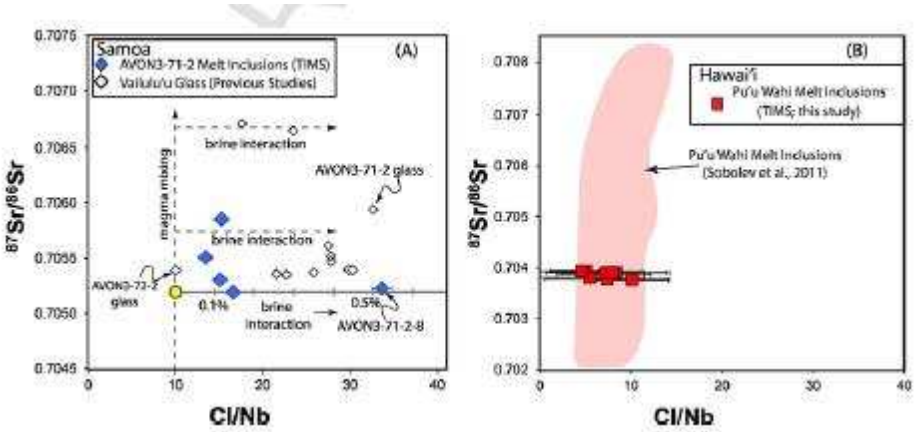

Figure 7

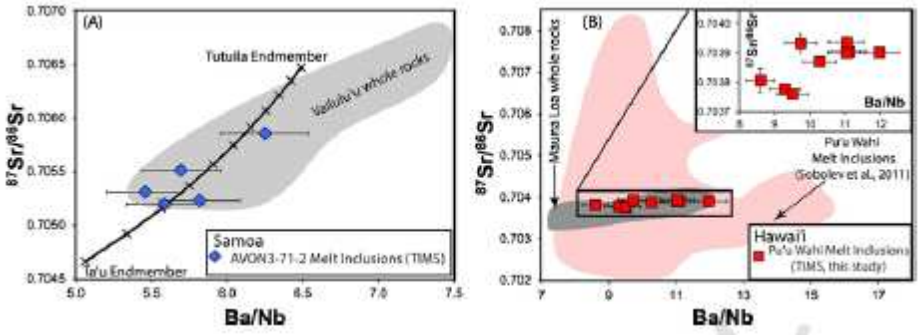

Figure 8

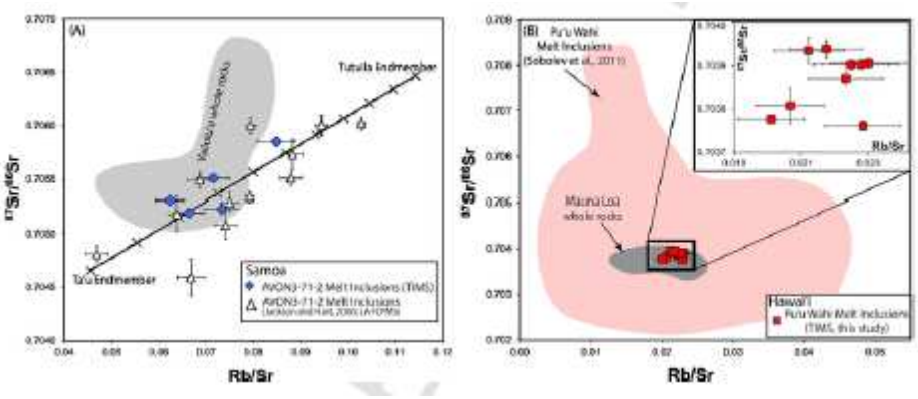

Figure 9

Figure captions

Fig. 1. Map of sample locations for A) the Hawaiian Puu Wahi flow on Mauna Loa and B) the Samoan sample AVON3-71-2 form Vailulu'u seamount. Panel C shows the Pacific region and the relative location of each sample. The base map imagery is from GeoMapApp (geomapapp.org).

Fig. 2. Olivine preparation schematic. Panel A is a photograph of a homogenized melt inclusion (AVON3-71-2-6) analyzed in this study (images of all melt inclusions are shown in Fig. S1). Prior to Sr and Nd isotopic analyses of melt inclusions, olivines with accessory inclusions were identified and accessory inclusions were removed (B), using a diamond wire saw to cut away portions of the olivine that contain accessory inclusions (C), then polishing away any remaining accessory inclusions (D), and finally exposing a small portion of the melt inclusion by polishing for EPMA, SIMS, and LA-ICPMS analyses (F). Panel E is an example of a melt inclusion (PW-1) that has been successfully isolated from accessory inclusions. Accessory inclusions include smaller melt inclusions, fluid inclusions, and spinel crystals.

Fig. 3. Major-element compositions of the Puu Wahi and AVON3-71-2 melt inclusions. Vailulu'u whole rock data are from Workman et al. (2004) and Jackson et al (2010). Mauna Loa whole rock data were taken from the Jackson et al. (2012) compilation of Hawaiian lavas, and only lavas with >6 wt% MgO are shown. Melt inclusion major elements are corrected for olivine crystallization to be in equilibrium with the host olivine, and are normalized to 100 wt.% totals (on a dry basis).

Fig. 4. Primitive mantle–normalized trace-element patterns from the seven glassy AVON3-71-2 melt inclusions and ten glassy Puu Wahi melt inclusions presented in this study (normalized to the primitive mantle values from McDonough and Sun, 1995). The black line is the trace-element data for the AVON3-71-2 whole rock from Workman et al. (2004), corrected for olivine accumulation to be in equilibrium with Fo_{90}. The grey line is the trace-element data for the host glass for the Puu Wahi olivines (Sobolev et al., 2011).

Fig. 5. All $^{87}Sr/^{86}Sr$ data published for AVON3-71-2 and Puu Wahi. In panel (A) $^{87}Sr/^{86}Sr$ data are presented for the AVON3-71-2 whole rock (Workman et al., 2004), melt inclusions by LA-MC-ICP-MS (Jackson and Hart, 2006), melt inclusions by TIMS (this study), clinopyroxene separates (separated by color; Jackson et al., 2009), and aggregated olivine (separated by color; Reinhard et al., 2016). The grey bar in (A) displays the total range of $^{87}Sr/^{86}Sr$ reported for Vailulu'u whole rocks by Workman et al. (2004), Jackson et al. (2010), and Jackson et al. (2014). For Puu Wahi, $^{87}Sr/^{86}Sr$ data for multi collector ICP-MS host glass (this study), laser ablation single-collector ICP-MS melt inclusion (Sobolev et al., 2011), and TIMS melt inclusion (this study) are also presented in panel (B). For the laser ablation-ICP-MS analyses of melt inclusions error bars are 2SE, for all other data the error bars are smaller than the symbols. The

grey bar in (B) displays the total $^{87}Sr/^{86}Sr$ variability reported in Mauna Loa whole rocks (compiled from the GEOROC database [http://georoc.mpch-mainz.gwdg.de]). The Puu Wahi host glass was analyzed as part of this study for $^{87}Sr/^{86}Sr$ (0.703912 ± 0.000008) and $^{143}Nd/^{144}Nd$ (0.512843±0.000006) using the methods described in Hart and Blusztajn (2006), and the Sr and Nd isotopic data are normalized to the preferred NBS 987 (0.710240) and JNdi (0.512104) ratios.

Fig. 6. $^{143}Nd/^{144}Nd$ versus $^{87}Sr/^{86}Sr$ for melt inclusions from Puu Wahi and AVON3-71-2. The grey field represents the global OIB array (compiled from the GEOROC database [http://georoc.mpch-mainz.gwdg.de]). Vailulu'u whole rock $^{87}Sr/^{86}Sr$ and $^{143}Nd/^{144}Nd$ data are from Workman et al. (2004), Jackson et al (2010), and Jackson et al. (2014). Mauna Loa whole rock $^{87}Sr/^{86}Sr$ and $^{143}Nd/^{144}Nd$ data were compiled from the GEOROC database [http://georoc.mpch-mainz.gwdg.de]. Grey squares with white stars are $^{143}Nd/^{144}Nd$ analyses on oceanic basalts from DePaolo and Wasserburg (1976; A is Mid-Atlantic Ridge MORB [VG295], B is Oahu nephelinite [HN-1], C is Oahu tholeiite [HT-1]), and the precision from these early whole rock $^{143}Nd/^{144}Nd$ analyses are similar to the precision obtained on individual melt inclusions in this study. All error bars are 2 SE. Melt inclusions with low Sr and Nd sample/blank ratios are not plotted (see Methods and Fig. S2).

Fig. 7. Cl/Nb plotted versus $^{87}Sr/^{86}Sr$ for AVON3-71-2 (A) and Puu Wahi (B). Vailulu'u glass $^{87}Sr/^{86}Sr$ and Cl/Nb data in (A) are from Workman et al. (2006) and Kendrick et al. (2015). Where a glass from Workman et al. (2004) was reanalyzed by the noble gas method for Cl by Kendrick et al. (2015), the Kendrick et al. (2015) value for Cl is used. The grey line with grey tick marks is a binary mixing model of a model melt (yellow circle; described in section 4.1.2.)

with a 55 wt% brine (as discussed in section 4.1.2.). Each tick mark represents 0.1% brine interaction. The vertical dashed line shows the effect of mixing the least contaminated (by seawater-derived materials) Vailulu'u melts and the horizontal dashed lines show the effect of interaction with brine . In (B) previously published Puu Wahi melt inclusion $^{87}Sr/^{86}Sr$ and Cl/Nb data (pale red field) from Sobolev et al. (2011) are plotted with the data from this study.

Fig. 8. $^{87}Sr/^{86}Sr$ versus Ba/Nb in the melt inclusions from AVON3-71-2 (A) and Puu Wahi (B). Vailulu'u whole rock $^{87}Sr/^{86}Sr$ and Ba/Nb field encompasses data from Workman et al. (2004), Jackson et al (2010), and Jackson et al. (2014). The black line is a mixing model between Ta'u lava T10 (from Workman et al., 2004 [0.704657; 437 ppm Sr, 19.9 ppm Rb, 178 ppm Ba, and 35.2 ppm Nb]) and Tutuila Island basalt sample TGH3-1931. Tic marks are 10% increments. TGH3-1931 (the enriched mixing endmember in the mixing model) was analyzed for trace elements and $^{87}Sr/^{86}Sr$ using the methods described in Hart and Blusztajn (2006). TGH3-1931 has 75.1 ppm Rb, 657 ppm Sr, 497 ppm Ba, 76.6 ppm Nb, and $^{87}Sr/^{87}Sr$ of 0.706467 (normalized to the preferred NBS 987 ratio of 0.710240). The AVON3-71-2 melt inclusion Ba/Nb and $^{87}Sr/^{86}Sr$ data from this study have a correlation coefficient of 0.81, however the p-value for this correlation is only 0.093, indicating the correlation is not significant at the 95% significance level. In (B), the Mauna Loa whole rock $^{87}Sr/^{86}Sr$ versus Ba/Nb field (from GeoRoc [http://georoc.mpch-mainz.gwdg.de]) compilation, encompasses the Puu Wahi melt inclusion analyses from this study; the inset shows a detailed view of Puu Wahi melt inclusions from this study.

Fig. 9. $^{87}Sr/^{86}Sr$ versus Rb/Sr for the AVON3-71-2 (A) and Puu Wahi (B) melt inclusions. In panel A, the open triangles are data from Jackson and Hart (2006). The black line is a binary

mixing line between the two endmembers (samples T10 and TGH-1931, see Fig. 8. caption), and tic ("X") marks are 10% mixing increments. The AVON3-71-2 melt inclusion Rb/Sr and $^{87}Sr/^{86}Sr$ data from this study give a correlation coefficient of 0.82 with a p-value of 0.087. The correlation coefficient of all AVON3-71-2 melt inclusion Rb/Sr and $^{87}Sr/^{86}Sr$ data from this study and the data of Jackson and Hart (2006) give a correlation coefficient of 0.79 with a p-value of 0.0002, indicating the correlation is significant at the 95% significance level. The R^2 for our model is 0.62; additionally, the residuals for our model show no correlation with Rb/Sr (correlation coeffieceint = -0.08). Vailulu'u whole rock $^{87}Sr/^{86}Sr$ and Ba/Nb data define a field that encompasses data from Workman et al. (2004) and Jackson et al (2010). In panel B, the field for Mauna Loa whole rock data encompasses data from the Jackson et al. (2012) compilation; a field for melt inclusion analyses from Sobolev et al. (2011) is also shown. The inset shows a detailed view of Puu Wahi melt inclusions from this study.

Acknowledgements.

We thank E. Gazel and an anonymous reviewer for constructive reviews, and C. Chauvel for editorial handling. MGJ acknowledges NSF grants OCE-1736984 and EAR-1624840. AAR gratefully acknowledges support from Ken MacDonald and Rachel Haymon through the UCSB Earth Science Department Graduate Opportunity Award which made this work possible.

References

Bach W., Peucker-Ehrenbrink B., Hart S. R., Blusztjan J. S., 2003. Geochemistry of hydrothermally altered oceanic crust: DSDP/ODP Hole 504B – Implications for seawater-crust exchange budgets and Sr- and Pb-isotopic evolution of the mantle. Geochem. Geophys. Geosyst. 4(3), 10.1029/2002GC000419

Beattie, P., 1994. Systematics and energetics of trace-element partitioning between olivine and

silicate melts: implications for the nature of mineral/melt partitioning. Chem. Geol. 117: 57-71

Bernat, M., Church, T., Allègre, C.J., 1972. Barium and strontium concentrations in Pacific and Mediterranean sea water profiles by direct isotope dilution mass spectrometry. Earth Planet. Sci. Lett. 16, 75–80.

Borisova A. Y., Faure F., Deloule E., Grègoire M., Bèjina F., de Parseval Ph. and Devidal J.-L., 2014. Lead isotope signatures of Kerguelen plume-derived olivine hosted melt inclusions: constraints on the ocean island basalt petrogenesis. Lithos 198–199, 153–171. http://dx.doi.org/10.1016/j.lithos.2014.03.022

Bryce, J.G., DePaolo, D.J., 2004. Pb isotopic heterogeneity in basaltic phenocrysts. Geochimica et Cosmochimica Acta 68, 4453–4468

Cabral, R.A., Jackson, M.G., Koga, K.T., Rose-Koga, E.F., Hauri, E.H., Whitehouse, M.J., Price, A.A., Day, J.M.D., Shimizu, N., Kelley, K.A., 2014. Volatile cycling of H_2O, CO_2, F, and Cl in the HIMU mantle: A new window provided by melt inclusions from oceanic hotspot lavas at Mangaia, Cook Islands. Geochemistry, Geophysics, Geosystems, 15. DOI: 10.1002/2014GC005473

Carlson, R.W., 1994. Mechanisms of earth differentiation - consequences for the chemical structure of the mantle. Rev. Geophys. 32, 337–361.

Charlou J. L., Donval J. P., Fouquet Y., Jean-Baptiste P. and Holm N. (2002) Geochemistry of high H2 and CH4 vent fluids issuing from ultramafic rocks at Rainbow hydrothermal field (36° 14'N, MAR). Chem. Geol. 191, 345–359.

Danyushevsky, L. V., Sobolev, A.V., Kononkova, N.N., 1992. Methods of studying melt inclusions in minerals during investigations on water-bearing primitive mantle melts (Tonga Trench boninites, Geochem. Int., 29, 48–62.

Danyushevsky, L. V., Della-Pasqua, F.N., Sokolov, S., 2000. Re-equilibration of melt inclusions trapped by magnesian olivine phenocrysts from subduction-related magmas: Petrological implications, Contrib. Mineral. Petrol., 138, 68–83

Danyushevsky, L.V., Perfit, M.R., Eggins, S.M., Falloon, T.J., 2003. Crustal origin for coupled 'ultra-depleted' and 'plagioclase' signatures in MORB olivine-hosted melt inclusions: evidence from the Siqueiros Transform Fault, East Pacific Rise. Contrib. Mineral. Petrol., 144, 619-637.

Danyushevsky, L.V., Leslie, R.A.J., Crawford, A.J., Durance, P., 2004. Melt inclusions in primitive olivine phenocrysts: the role of localized reaction processes in the origin of anomalous compositions. J. Pet., 45, 2531–2553.

DePaolo, D., Wasserburg, G.J., 1976. Inferences about magma sources and mantle structure from variations of $^{143}Nd/^{144}Nd$. Geophys. Res. Lett., 3, 743-746.

Fontignie, D., Schilling, J.G., 1996. Mantle heterogeneities beneath the South Atlantic: a Nd–Sr–Pb isotope study along the Mid-Atlantic Ridge (3°S–46°S). Earth Planetary Science Letters 142, 209–221Ford et al., 1983

Fujimaki, H., Tatsumoto, M. and Aoki, K.-i., 1984. Partition coefficients of Hf, Zr, and REE between phenocrysts and groundmasses. Journal of Geophysical Research 89: 662-672.

Gaetani, G.A., Watson, E.B., 2000. Open system behavior of olivine hosted melt inclusions. Earth Planet. Sci. Lett. 183, 27 – 41.

Gaetani, G.A., O'Leary, J.A., Shimizu, N., Bucholz, C.E., Newville, M, 2012. Rapid re-equilibration of H2O and oxygen fugacity in olivine-hosted melt inclusions. Geology, 40, 915–918, http://dx.doi.org/10.1130/G32992.1.

Gagnon J. E., Fryer B. J., Samson I. M. and Williams-Jones A. E., 2008. Quantitative analysis of silicate certified reference materials by LA-ICPMS with and without an internal standard. J. Anal. At. Spectrom. 23, 1529–1537

Gast, P.W., Tilton, G.R., Hedge, C., 1964. Isotopic composition of lead and strontium from Ascension and Gough Islands. Science, 145, 1181-1185.

Gurenko, A. A., Chaussidon, M., 1995. Enriched and depleted primitive melts in olivine from Icelandic tholeiites: Origin by continuous melting of a single mantle column. Geochim. Cosmochim. Acta, 59, 2905-2917.

Harlou, R., Pearson, D.G., Nowell, G.M., Ottley, C.J., Davidson, J.P., 2009. Combined Sr isotope and trace element analysis of melt inclusions at sub-ng levels using micro-milling, TIMS and ICPMS. Chem. Geol. 260, 254–268.

Hart, S.R., Blusztajn, J., 2006. Age and geochemistry of the mafic sills, ODP site 1276, Newfoundland margin. Chemical Geology 235, 222-237.

Hauff, F., Hoernle, K., Schmidt, A., 2003. Sr-Nd-Pb composition of Mesozoic Pacific oceanic crust (Site 1149 and 801, ODP Leg 185): Implications for alteration of ocean crust and the input into the Izu-Bonin-Mariana subduction system. Geochem. Geophys. Geosyst. 4, 8913 DOI:10.1029/2002GC000421

Hofmann, A. W., White, W.M., 1982. Mantle plumes from ancient oceanic crust. Earth Planet. Sci. Lett. 57, 421-436.

Hofmann, A.W., 1997. Mantle geochemistry: the message from oceanic volcanism. Nature, 385, 219-229.

Jackson, M.G., Hart, S.R., 2006. Strontium isotopes in melt inclusions from Samoan basalts: Implications for heterogeneity in the Samoan plume. Earth Planet. Sci. Lett. 245, 260-277.

Jackson, M.G., Hart, S.R., Koppers, A.A.P., Staudigel, H., Konter, J., Blusztajn, J., Kurz, M.D.,

Russell, J.A., 2007. The return of subducted continental crust in Samoan lavas. Nature, 448, 684-687.

Jackson, M.G., Hart, S.R., Shimizu, N., Blusztajn, J., 2009. Pervasive cpx-whole rock isotopic disequilibrium in Polynesian hotspot lavas: Evidence supporting isotopic variability in olivine and clinopyroxene-hosted melt inclusions. Geochem. Geophys. Geosys. 10, Q03006, doi:10.1029/2008GC002324

Jackson, M.G., Hart, S.R., Konter, J.P., Koppers, A.A.P., Staudigel, H., Kurz, M.D., Blusztajn, J., Sinton, J.M., 2010. The Samoan hotspot track on a "hotspot highway": Implications for mantle plumes and a deep Samoan mantle source. Geochem. Geophys. Geosyst. 11, Q12009, doi:10.1029/2010GC003232

Jackson, M.G., Shirey, S., 2011. Re-Os systematics in Samoan shield lavas and the use of Os-isotopes in olivine phenocrysts to determine primary magmatic compositions. Earth Planet. Sci. Lett. 312, 91-101.

Jackson M. G., Weis, D., Huang, S., 2012. Major element variations in Hawaiian shield lavas: source features and perspectives from global ocean island basalt (OIB) systematics. Geochem. Geophys. Geosyst. 13, Q09009. http://dx.doi.org/ 10.1029/2012GC004268

Jackson, M.G., Carlson, R.W., 2012. Homogeneous superchondritic 142Nd/144Nd in the mid-ocean ridge basalt and ocean Island basalt mantle. Geochem. Geophys. Geosyst.13, Q06011. https://doi.org/10.1029/2012GC004114.

Jackson, M.G., Hart, S.R., Konter, J.G., Kurz, M.D., Blusztajn, J., Farley, K., 2014. Helium and lead isotopes reveal the geochemical geometry of the Samoan plume. Nature, 514, 355-358.

Jambon, A., Deruelle, B., Dreibus, G., Pineau, F., 1995. Chlorine and bromine abundance in MORB: The contrasting behaviour of the Mid-Atlantic Ridge and East Pacific Rise and implications for chlorine geodynamic cycle. Chem. Geol., 126, 101–117.

Jochum K., Stoll B., Herwig K., Willbold M., Hofmann A., Amini M., Aarburg S., Abouchami W., Hellebrand E., Mocek B., Raczek I., Stracke A., Alard O., Bouman C., Becker S., Du¨cking M., Bra¨tz H., Klemd R., Bruin D., Canil D., Cornell D., Hoog C.-J., Dalpe´ C., Danyushevsky L., Eisenhauer A., Gao Y., Snow J., Groschopf N., Gu¨nther D., Latkoczy C., Guillong M., Hauri E., Ho¨fer H., Lahaye Y., Horz K., Jacob D., Kasemann S., Kent A., Ludwig T., Zack T., Mason P., Meixner A., Rosner M., Misawa K., Nash B., Pfa¨nder J., Premo W., Sun W., Tiepolo M., Vannucci R., Vennemann T., Wayne D. and Woodhead J., 2006. MPI-DING reference glasses for in situ microanalysis: New reference values for element concentrations and isotope ratios. Geophys. Geosyst., 7

Jochum K.P., Nohl U., 2008. Reference materials in geochemistry and environmental research and the GeoReM database. Chemical Geology, 253, 50-53.

Kamenetsky, V.S., Eggins, S.M., Crawford, A.J., Green, D.H., Gasparon, M., Falloon, T.J., 1998. Calcic melt inclusions in primitive olivine at 43° N MAR: evidence for melt–rock reaction/melting involving clinopyroxene-rich lithologies during MORB generation. Earth Planet. Sci. Lett., 160, 115–132.

Kelley, K.A., Plank, T., Ludden, J., Staudigel, H., 2003. Composition of altered oceanic crust at ODP Sites 801 and 1149. Geochemisty, Geophysics, Geosystems, 4, doi:10.1029/2002GC000435

Kelley, K. A., Kingsley, R., Schilling, J.-G., 2013, Composition of plume-influenced mid-ocean ridge lavas and glasses from the Mid-Atlantic Ridge, East Pacific Rise, Galapagos Spreading Center, and Gulf of Aden, Geochem. Geophys. Geosyst., 14, 223-242, doi:10.1029/ 2012GC004415

Kendrick, M.A., Arculus, R., Burnard, P., Honda, M., 2013. Quantifying brine assimilation by submarine magmas: Examples from the Galapagos Spreading Centre and Lau Basin. Geochim. Cosmochim. Acta, 123, 150–165. doi:10.1016/j.gca.2013.09.012.

Kendrick, M.A., Jackson, M.G., Kent, A.J.R., Hauri, E.H., Wallace, P.J., Woodhead, J., 2014. Contrasting behaviors of CO_2, S, H_2O and halogens (F, Cl, Br, and I) in enriched-mantle melts from Pitcairn and Society seamounts. Chem. Geol., 370, 69-81.

Kendrick, M.A., Jackson, M.G., Hauri, E.H., Phillips, D., 2015. The halogen (F, Cl, Br, I) and H_2O systematics of Samoan lavas: assimilated-seawater, EM2 and high-$^3He/^4He$ components. Earth Planet. Sci. Lett., 410, 197-209.

Kent, A.J., Norman, M.D., Hutcheon, I.D., Stolper, E.M., 1999a. Assimilation of seawater-derived components in an oceanic volcano: Evidence from matrix glasses and glass inclusions from Loihi seamount, Hawaii. Chem. Geol., 156, 299–319.

Kent, A.J., Clague, D.A., Honda, M., Stolper, E.M., Hutcheon, I.D., Norman, M.D., 1999b. Widespread assimilation of a seawater-derived component at Loihi Seamount, Hawaii. Geochim. Cosmochim. Acta, 63, 2749–2761.

Kent, A.J.R., Baker, J.A., Wiedenbeck, M., 2002. Contamination and melt aggregation processes in continental flood basalts: constraints from melt inclusions in Oligocene basalts from Yemen. Earth Planet. Sci. Lett., 202, 577-594

Kent, A.J.R., 2008. Melt Inclusions in Basaltic and related Volcanic rocks. Reviews in Mineralogy & Geochemistry, 69, 273-331

Knaf, A.C.S., Koornneef, J.M., Davies, G.R., 2017. "Non-invasive" portable laser ablation sampling of art and archaeological materials with subsequent Sr–Nd isotope analysis by TIMS using 10^{13} Ω amplifiers. J. Anal. Atomic Spectrometry, 32, 2210-2216

Koornneef, J.M., Bouman, C., Schwieters, J.B., Davies, G.R., 2014. Measurement of small ion beams by thermal ionization mass spectrometry using new 10^{13} Ohm resistors. Analytica Chimica Acta, 819, 49-55.

Koornneef, J.M., Nikogosian, I., van Bergen, M.J., Smeets, R., Bouman, C., Davies, G.R., 2015. TIMS analysis of Sr and Nd isotopes in melt inclusions from Italian potassium-rich lavas using prototype 10^{13} Ω amplifiers. Chem. Geol. 397, 14-23.

Lassiter, J.C., Hauri, E.H., Nikogosian, I.K., Barsczus, H.G., 2002. Chlorine–potassium variations in melt inclusions from Raivavae and Rapa, Austral Islands: Constraints on chlorine recycling in the mantle and evidence for brine-induced melting of oceanic crust. Earth Planet. Sci. Lett., 202, 525–540.

le Roux, P.J., Shirey, S.B., Hauri, E.H., Perfit, M.R., Bender, J.F., 2006. The effects of variable sources, processes and contaminants on the composition of northern EPR MORB (8–10°N and 12–14°N): evidence from volatiles (H_2O, CO_2, S) and halogens (F, Cl). Earth and Planetary Science Letters 251, 209–231.

Le Voyer, M., Rose-Koga, E.F., Laubier, M., Schiano, P., 2008. Petrogenesis of arc lavas from the Rucu Pichincha and Pan de Azucar volcanoes (Ecuadorian arc): Major, trace element, and boron isotope evidences from olivine-hosted melt inclusions. Geochem. Geophys. Geosyst. 9, http://dx.doi.org/10.1029/2008GC002173.

Lockwood, J.P., 1995. Mauna Loa eruptive history: The preliminary radiocarbon record, in Rhodes, J.M., and Lockwood, J.P., eds., Mauna Loa Revealed: Structure, Composition, History, and Hazards: American Geophysical Union Geophysical Monograph 92, p. 81–94, doi:10.1029/GM092p0081

Maclennan, J., McKenzie, D., Granvold, K., Shimizu, N., Eiler, J.M., Kitchen, N., 2003a. Melt mixing and crystallization under Theistareykir, northeast Iceland. Geochem. Geophys. Geosyst., 4. doi:10.1029/2003GC000558

Maclennan J., McKenzie, D., Hilton, D., Granvold, K., Shimizu, N., 2003b. Geochemical variability in a single flow from northern Iceland. J. Geophys. Res., 108, 2007.

Maclennan, J., 2008. Lead isotope variability in olivine-hosted melt inclusions from Iceland, Geochim. Cosmochim. Acta 72, 4159–4176.

McDonough, W.F., Sun, S.S., 1995. The composition of the Earth. Chem. Geol. 120, 223–253.

Melson, W. G., O'Hearn, T., Jarosewich, E., 2002. A data brief on the Smithsonian Abyssal Volcanic Glass Data File, Geochem. Geophys. Geosyst., 3(4), 1023, doi:10.1029/ 2001GC000249.

Michael, P.J., Cornell, W.C., 1998. Influence of spreading rate and magma supply on crystallization and assimilation beneath mid-ocean ridges: Evidence from chlorine and major element chemistry of mid-ocean ridge basalts. J. Geophys. Res., 103, 18,325-18,356.

Mokadem F., Parkinson, I.J., Hathorne, E.C., Anand, P., Allen, J.T., Burton, K.W., 2015. High-precision radiogenic strontium isotope measurements of the modern and glacial ocean: limits on glacial–interglacial variations in continental weathering. Earth Planet. Sci. Lett. 415, 111–120.staud

Oulton, J., Humayun, M., Fedkin, A., Grossman, L., 2016. Chemical evidence for differentiation, evaporation and recondensation from silicate clasts in Gujba, Geochim. Cosmochim. Acta, 177, 254-274.

Reinhard, A.A., Jackson, M.G., Harvey, J., Brown, C., Koornneef, J.M., 2016. Extreme differences in $^{87}Sr/^{86}Sr$ between magmatic olivines and Samoan host lavas: Evidence for highly heterogeneous $^{87}Sr/^{86}Sr$ in the magmatic plumbing system sourcing a single lava. Chem. Geol. 438, 120-131.

Remmert P., Dohmen R., Chakraborty S., 2008. Diffusion of REE, Hf and Sr in olivine. Eos Trans. AGU, 89(53) Fall Meet. Suppl. MR33A-1844 (abstr.)

Roeder, P.L., Emslie, R.F., 1970. Olivine–liquid equilibrium. Contribution to Mineralogy and Petrology 29, 275–289.

Rose-Koga, E.F., Koga, K., Schiano, P., Le Voyer, M., 2012. Mantle source heterogeneity for South Tyrrhenian magmas revealed by Pb isotopes and halogen contents of olivine-hosted melt inclusions. Chem. Geol., 334, 266-279

Rose-Koga E., Koga K., Moreira, M., Vlastélic, I., Jackson, M.G., Whitehouse, M.J., Shimizu, N., Habib, N., 2017. Geochemical systematics of Pb isotopes, fluorine, and sulfur in melt inclusions from São Miguel, Azores. Chemical Geology vol.458, p.22-37, doi:10.1016/j.chemgeo.2017.03.024.

Rowe, M.C., Lassiter, J.C., 2009. Chlorine enrichment in central Rio Grande Rift basaltic melt inclusions: Evidence for subduction modification of the lithospheric mantle. Geology, 37, 439-442.

Rowe, M.C., Lassiter, J.C., Goff, K., 2015. Basalt volatile fluctuations during continental rifting: an example from the Rio Grande Rift, USA. Geochem. Geophys. Geosyst. 16. http://dx.doi.org/10.1002/2014GC005649.

Saal, A.E., Hart, S.R., Shimizu, N., Hauri, E.H., Layne, G.D., 1998. Pb isotopic variability in

melt inclusions from oceanic island basalts, Polynesia. Science 282:1481-1484.

Saal, A.E., Hauri, E.H., Langmuir, C.H., Perfit, M.R., 2002. Vapour undersaturation in primitive mid-ocean-ridge basalt and the volatile content of Earth's upper mantle. Nature, 419, 451- 455.

Saal, A.E., Hart, S.R., Shimizu, N., Hauri, E.H., Layne, G.D., Eiler, J.M., 2005. Pb isotopic variability in melt inclusions from the EMI-EMII-HIMU mantle end-members and the role of oceanic lithosphere. Earth Planet. Sci. Lett. 240:605–20.

Saal, A.E., Kurz, M.D., Hart, S.R., Blusztajn, J.S., Blichert-Toft, J., Liang, Y., Geist, D.J., 2007. The role of lithospheric gabbros on the composition of Galapagos lavas. Earth Planet. Sci. Lett. 257 (3–4), 391–406.

Salters, V.J.M., Mallick, S., Hart, S.R., Langmuir, C.E., Stracke, A., 2011. Domains of depleted mantle: New evidence from hafnium and neodymium isotopes. Geochem. Geophys. Geosyst., 12, Q08001, doi:10.1029/2011GC003617.

Sakyi, P. A., Tanaka, R., Kobayashi, K., Nakamura, E., 2012. Inherited Pb isotopic record in olivine antecryst-hosted melt inclusions from Hawaiian lavas. Geochim. Cosmochim. Acta 95, 169–195.

Sano, T., Miyoshi, M., Ingle, S., Banerjee, N.R., Ishimoto, M., Fukuoka, T., 2008. Boron and chlorine contents of upper oceanic crust: Basement samples from IODP Hole 1256D. Geochem. Geophys. Geosyst., 9, Q12O15. doi:10.1029/2008GC002182

Schilling, J. G., Hanan, B. B., McCully, B., Kingsley, R.H., Fontignie, D., 1994. Influence of the Sierra Leone mantle plume on the equatorial Mid-Atlantic Ridge: A Nd-Sr-Pb isotopic study, J. Geophys. Res., 99(B6), 12,005–12,028, doi:10.1029/94JB00337.

Schmidt, K., Koschinsky, A., Garbe-Schönberg, D., de Carvalho, L.M., Seifert, R., 2007. Geochemistry of hydrothermal fluids from the ultramafic-hosted Logatchev I hydrothermal field, 15°N on the Mid-Atlantic Ridge: Temporal and spatial investigation, Chem. Geol., 242(1–2), 1–21, doi:10.1016/j.chemgeo.2007.01.023.

Sims, K.W.W., Hart, S.R., Reagan, M.K., Blusztajn, J., Staudigel, H., Sohn, R.A., Layne, G.D., Ball, L.A., 2008. ^{238}U-^{230}Th-^{226}Ra-^{210}Pb-^{210}Po, ^{232}Th-^{228}Ra, and ^{235}U-^{231}Pa constraints on the ages and petrogenesis of Vailulu'u and Malumalu Lavas, Samoa. Geochem. Geophys. Geosyst., 9. Q04003, doi:10.1029/2007GC001651.

Sobolev, A.V., Shimizu, N., 1993. Ultra-depleted primary melt included in an olivine from the mid-Atlantic ridge. Nature, 363, 151-154.

Sobolev A.V., and Danyushevsky L.V. (1994). Petrology and geochemistry of boninites from the north termination of the Tonga Trench: constraints on the generation conditions of primary high-Ca boninite magmas. Journal of Petrology, 35, 1183-1213.

Sobolev, A.V., Hofmann, A.W., Nikogosian. I.K., 2000. Recycled oceanic crust observed in 'ghost plagioclase' within the source of Mauna Loa lavas. Nature, 404, 986-990.

Sobolev, A.V., Hofmann, A.W., Jochum, K.P., Kuzmin, D.V., Stoll, B., 2011. A young source for the Hawaiian plume. Nature, 476, 434–437.

Staudigel, H., Davies, G.R., Hart, S.R., Marchant, K.M., Smith, B.M., 1995. Large scale isotopic Sr, Nd and O isotopic anatomy of altered oceanic crust: DSDP/ODP sites 417/418. Earth Planet. Sci. Lett, 130, 169-185.

Staudigel, H., Plank, T., White, B., Schminke, H.-U., 1996. Geochemical fluxes during seafloor alteration of the basaltic upper oceanic crust: DSDP Sites 417 and 418, in Subduction: Top to Bottom, Geophys. Monogr. Ser., vol. 96, edited by G. E. Bebout et al., pp. 19-38, AGU, Washington, D.C., 1996.

Staudigel, H., 2003. Hydrothermal Alteration Processes in the Oceanic Crust. Treatise on Geochemistry, 3, 511-535.

Stracke, A., 2016. Mantle Geochemistry. Encyclopedia of Geochemistry, p. 12. doi: DOI 10.1007/978-3-319-39193-9_286-1.

Stroncik, N.A., Haase, K.M., 2004. Chlorine in oceanic intraplate basalts: Constraints on mantle sources and recycling processes. Geology 32, 945. doi:10.1130/G21027.1.

Tanaka, T., Togashi, S., Kamioka, H., Dragusanu, C., 2000. JNdi-1: A neodymium isotopic reference in consistency with La Jolla neodymium, Chem. Geol., 168, 279–281.

Thirlwall, M.F., 1991. Long-term reproducibility of multicollector Sr and Nd isotope ratio analysis. Chem. Geol. 94, 85–104.

Van den Bleeken, G., Koga, K.T., 2015. Experimentally determined distribution of fluorine and chlorine upon hydrous slab melting, and implications for F–Cl cycling through subduction zones. Geochim. Cosmochim. Acta 171, 353–373

Vroon, P.Z., van der Wagt, B., Koornneef, J.M., Davies, G.R., 2008. Problems in obtaining precise and accurate Sr isotope analysis from geological materials using laser ablation MC - ICPMS. Anal. Bioanal. Chem. 390, 465-476.

Wallace, P.J., Kamenetsky, V.S., Cervantes, P., 2015. Melt inclusion CO2 contents, pressures of olivine crystallization, and the problem of shrinkage bubbles. Am. Mineral. 100 (4), 787–794

Weis, D., Kieffer, B., Maerschalk, C., Barling, J., Jong, J.D., Williams, G.A., Hanano, D.,Pretorius, W., Mattielli, N., Scoates, J.S., Goolaerts, A., Friedman, R.M., Mahoney, J.B., 2006. High precision isotopic characterization of USGS reference materials by TIMS and MC-ICP-MS. Geochem. Geophys. Geosyst. 7 (8), 139–149

White, W. M., 1985. Source of oceanic basalts: Radiogenic isotopic evidence, Geology 13, 115–118.

White, W. M., 2010. Oceanic Island Basalts and mantle plumes: The geochemical perspective. Annu. Rev. Earth Planet. Sci. Lett. 38, 133–160.

White, W.M., 2015a. Isotopes, DUPAL, LLSVPs, and Anekantavada. Chem. Geol. 419, 10-28.

White, W. M., 2015b. Probing the Earth's Deep Interior Through Geochemistry. Geochemical Perspectives 4 (2): 95-251

Workman, R.K., Hart, S.R., Jackson, M.G., Regelous, M., Farley, K.A., Blusztajn, J., Kurz, M.D., 2004. Recycled metasomatised lithosphere as the origin of the Enriched Mantle II (EM2) end-member: Evidence from the Samoan Volcanic Chain. Geochem. Geophys. Geosys., 5gao, doi:10.1029/2003GC000623.

Workman, R.K., Hauri, E., Hart, S.R., Wang, J., Blusztajn, J., 2006. Volatile and trace elements in basaltic glasses from Samoa: Implications for water distribution in the mantle. Earth Planet. Sci. Lett., 241, 932–951.

Workman, R.K., Hart, S.R., Eiler, J.M., Jackson, M.G., 2008. Oxygen isotopes in Samoan lavas: confirmation of continent recycling. Geology, 36, 551-554.

Yurimoto, H., Kogiso, T., Abe, K., Barsczus, H.G., Utsunomiya, A., Maruyama, S., 2004. Lead isotopic compositions in olivine-hosted melt inclusions from HIMU basalts and possible link to sulfide components, Phys. Earth Planet. Inter.,146(1–2), 231–242, doi:10.1016/j.pepi.2003.08.013

Zindler, A., Hart, S.R., 1986. Chemical geodynamics. Annu. Rev. Earth Planet. Sci., 14, 493–571.

Supplementary Material

1. Supplementary Methods

Volatile Measurements

Volatile element (CO_2, H_2O and F) concentrations were measured on the Cameca 1280-HR SIMS at CRPG-CNRS-Nancy (France). The analytical procedures are detailed in other studies (e.g. Rose-Koga et al., 2014) and are summarized briefly here. A Cs^+ primary ion beam

was used with a nominal current of 0.7 nA, a 10 kV secondary accelerating voltage, and a -80 V offset. An electron gun was used to compensate for charge buildup on the sample. The instrument was operated with the contrast aperture at 400 μm, and the energy aperture was set at 30 eV. The entrance slit was set to 122 μm and the exit slit to 173 μm, for a mass resolution power of 7007. The pre-sputter was set to 3 minutes. During each analysis, background was measured (2 s), followed by measurement of ^{12}C (8 s), ^{17}O (3 s), $^{16}O^{1}H$ (6 s), ^{18}O (3s), ^{19}F (4 s), ^{27}Al (3 s), and ^{30}Si (3 s); there was a two-second delay after each magnet shift. This cycle was repeated 10 times during each analysis, yielding a total measurement time (including pre-sputter) of between ten and eleven minutes per spot. A ^{12}C ion image of each melt inclusion was examined prior to analysis to avoid portions of melt inclusions with C surface contamination, and sample analyses that exhibit drift in $^{12}C/^{30}Si$ during an analysis were discarded.

Calibration curves for H_2O, CO_2 and F were generated by measuring basaltic glass reference materials (VG2, M40, M48, N272, and A99). ALV 519-4-1 (volatile concentrations are reported in Hauri, 2002; and Kumamoto et al., 2017) and GL07 D52-5 (summarized in Jackson et al., 2015 and Simons et al., 2002) were run as secondary standards. The analytical errors, which are based on the reproducibility over the 10 cycles of analyses of geological reference materials (Table S2) and the errors on the regression of the calibration line were <5 % for H_2O, <15 % for CO_2, and 5 % for F (1 RSD).

2. Supplementary Observations

CO_2 and H_2O in melt inclusions.

CO_2 concentrations measured in the melt inclusion glass from AVON3-71-2 (373–719 ppm; Table S6) are higher than values measured in submarine pillow rim glass from Vailulu'u (6–233 ppm; Workman et al., 2006), and overlap with the range of CO_2 concentrations previously reported in olivine-hosted melt inclusions from Vailulu'u (53–515 ppm; Workman et

al., 2006) (Fig. S3). H_2O concentrations in the AVON3-71-2 melt inclusions (0.95- 1.33 wt. %; Table S6) fall within the range of previously analyzed pillow rim glasses (0.63 – 1.50 wt. %) and melt inclusions (0.67 – 1.48 wt. %) from Vailulu'u (Workman et al., 2006).

The Puu Wahi melt inclusions span the same range of H_2O concentrations (0.29–0.34 wt. %; see Fig. S3 and Table S6) as a different suite of unheated melt inclusions from the same sample analyzed by Wallace et al. (2015). With one exception, the unheated (25-207 ppm, n=7) and reheated (54 to 122 ppm, n=2) Puu Wahi melt inclusions from our study have relatively low CO_2 concentrations that are consistent with the range in CO_2 concentrations measured in unheated melt inclusions from the same sample analyzed by Wallace et al. (2015; 38-158 ppm). One Puu Wahi melt inclusion that was not homogenized has a CO_2 concentration (520 ppm) that is similar to the heated melt inclusions analyzed by Wallace et al. (2015), which range from 224 to 505 ppm CO_2. The suite of melt inclusions from the same sample analyzed by Wallace et al. (2015) showed that melt inclusions often host a large portion of their CO_2 (40–90%) in vapor bubbles, and that over-heating followed by rapid quenching is required to re-dissolve the CO_2 hosted in the vapor bubble. The melt inclusions in our study were not overheated and most had visible vapor bubbles after homogenization that represented up to 5% of the volume of the melt inclusion (Fig. S4). Previous studies (Steele-MacInnis et al. 2011; Moore et al., 2015; Wallace et al., 2015) have shown that a significant portion of the CO_2 in the melt inclusion may be hosted in the vapor bubble, and the concentrations measured in the glassy portion of the melt inclusions are not representative of the original trapped melt. Because we did not overheat the Puu Wahi (or Vailulu'u) melt inclusions to re-dissolve the vapor bubble, we do not further discuss CO_2 concentrations in this study.

3. Supplementary Discussion

Assimilation of oceanic crust: deep crustal gabbros or shallow altered crust. The data from the AVON3-71-2 melt inclusions do not support the assimilation of deep oceanic crust generating $^{87}Sr/^{86}Sr$ heterogeneity. Previous work has shown that, in contrast to shallow oceanic crust, deep oceanic crust is often not altered (Staudigel et al., 1995, 1996; Hart et al., 1999), particularly the deep gabbro section of crust generated at fast-spreading ridges (Gao et al., 2016) (a spreading rate regime that is likely applicable to the formation of the oceanic crust beneath Samoa; Muller et al., 2008). Thus, assimilation of deep oceanic crust is not expected to influence the Cl/Nb ratios of basalts. However, deep oceanic crust is dominated by gabbros, which should impart a "plagioclase" trace element signature on a pristine melt that assimilates lower oceanic crust (Saal et al., 2007; Peterson et al., 2014). Positive Sr anomalies can be used as an indicator of plagioclase assimilation, where enrichment in Sr relative to Nd and Sm, or Sr/Sr*>1, is used as the definition of a positive Sr anomaly (i.e., $Sr/Sr^*=Sr_N/(Sm_N*Nd_N)^{0.5}$). Therefore, assuming oceanic gabbro has MORB-like $^{87}Sr/^{86}Sr$ (0.7028; Gale et al., 2013), gabbro assimilation by Samoan melts would result in a reduction in melt inclusion $^{87}Sr/^{86}Sr$ with a concomitant increase in Sr/Sr* values. However, all AVON3-71-2 melt inclusions have Sr/Sr* ≤ 1.03 and show no correlation between $^{87}Sr/^{86}Sr$ and Sr/Sr* (Fig. S5), and the data are therefore inconsistent with the magma having assimilated oceanic crustal gabbros.

Similarly, the data from the AVON3-71-2 melt inclusions analyzed in this study are not consistent with assimilation of AOC as the mechanism generating $^{87}Sr/^{86}Sr$ heterogeneity. In highly altered 167 Ma (ODP site 801) and 130 Ma (ODP site 1149) oceanic crust, Hauff et al. (2003) found the average $^{87}Sr/^{86}Sr$ of the igneous portions to be 0.704947 and 0.704769, respectively, values that are similar to the average $^{87}Sr/^{86}Sr$ of 120 Ma altered oceanic crust from ODP sites 417/418 of 0.704575 (Staudigel et al., 1995). These altered oceanic crust drill cores sample crust with $^{87}Sr/^{86}Sr$ values that are lower than any whole rock or glass $^{87}Sr/^{86}Sr$ from

Vailulu'u volcano (Workman et al., 2004, 2006; Jackson et al., 2010, 2014) and lower than all of the AVON3-71-2 melt inclusions analyzed here. Therefore, the assimilation of altered oceanic crust should result in a reduction of the $^{87}Sr/^{86}Sr$ of any Vailulu'u melts while increasing Cl/Nb ratios, resulting in a negatively sloping trend. Such a trend is not observed in the AVON3-71-2 melt inclusion suite in Figure 7, arguing against assimilation of altered oceanic crust as the mechanism driving $^{87}Sr/^{86}Sr$ variability in AVON3-71-2 melt inclusions.

Hauff et al. (2003) found that some components in the basement portion of ODP core 801, including calcite-, smectite-, and hyaloclastite-rich materials, can have extremely radiogenic $^{87}Sr/^{86}Sr$ (up to 0.7257 in sample 801C 17R4 15-18 from Hauff et al., 2003). The highest $^{87}Sr/^{86}Sr$ samples from ODP core 801 exhibit enrichments in Rb and K (Kelley et al., 2003), as expected in altered oceanic crust (Staudigel, 2003; Sano et al., 2008). If the $^{87}Sr/^{86}Sr$ heterogeneity in Samoan melt inclusions is due to assimilation of this extreme oceanic crust composition, and if we assume that the highest $^{87}Sr/^{86}Sr$ melt inclusion from AVON3-71-2 (0.705853, AVON3-71-2-3) is the result of incorporation of altered oceanic crust by a melt similar to the lowest $^{87}Sr/^{86}Sr$ melt inclusion (AVON3-71-2-9, 0.705193), then approximately 33% altered oceanic crust (with a composition like the drill core sample 801C 17R4 15-18) would have to be assimilated. Such large quantities of assimilated material will modify the major and trace element composition of the high $^{87}Sr/^{86}Sr$ melt inclusion: if a melt similar to melt inclusion AVON3-71-2-9 is mixed with 33% of the highly radiogenic $^{87}Sr/^{86}Sr$ drill core sample (801C 17R4 15-18 from Hauff et al., 2003), the melt resulting from assimilation would have significant enrichments in Rb and K relative to the AVON3-71-2 melt inclusions (see the AOC assimilation model in Fig. S6). Also, as the highly radiogenic $^{87}Sr/^{86}Sr$ sample is carbonate-rich (Hauff et al., 2003) and has 27.3 % CaO, the resulting assimilated melt would have ~16.2 wt. % CaO (at ~9.5 wt. % MgO), nearly 40 % more CaO than the highest CaO AVON3-71-2 melt

inclusion (11.7 wt. %) (note that the assimilated melt has such high CaO that it plots outside of the relevant panel in Fig. 3). The lack of enrichments in Rb, K, Ca in the highest $^{87}Sr/^{86}Sr$ melt inclusion (AVON3-71-2-3) argues against the assimilation of highly radiogenic $^{87}Sr/^{86}Sr$ components of AOC.

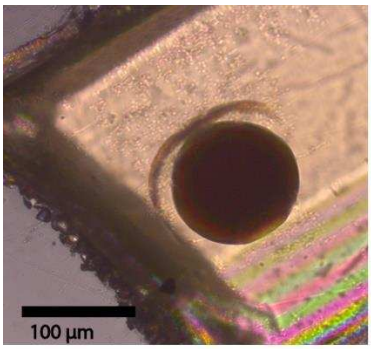

Melt inclusion PW1

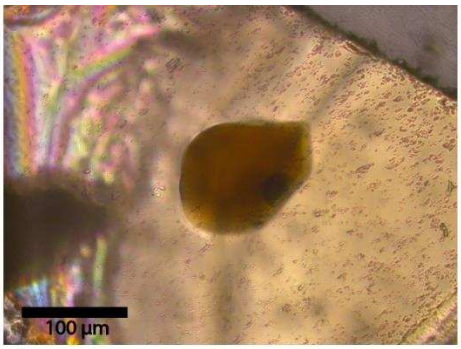

Melt inclusion PW2

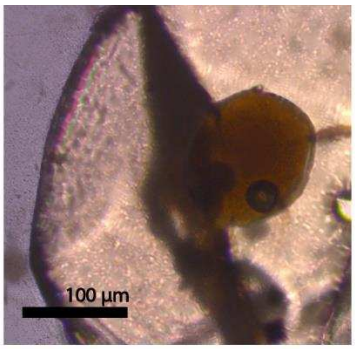

Melt inclusion PW3

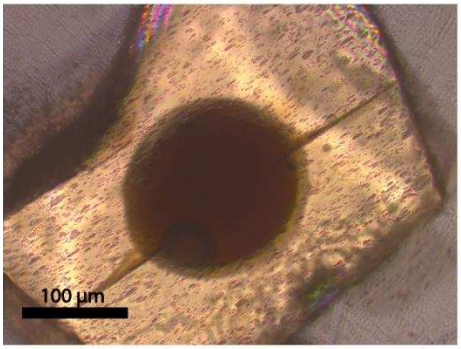

Melt inclusion PW4

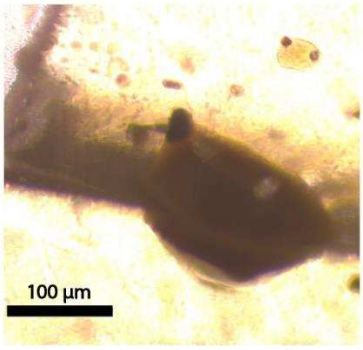

Melt inclusion PW5

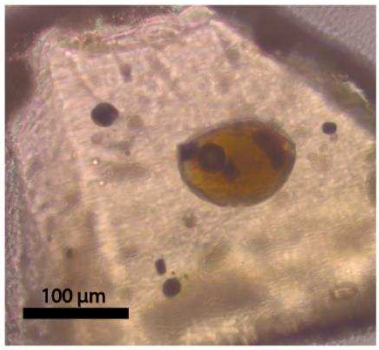

Melt inclusion PW6

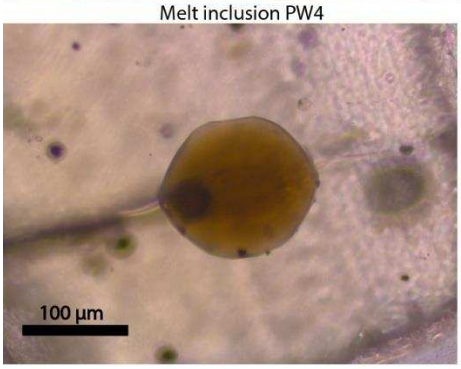

Melt inclusion PW8

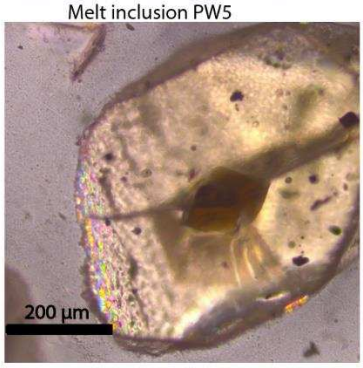

Melt inclusion PW9a

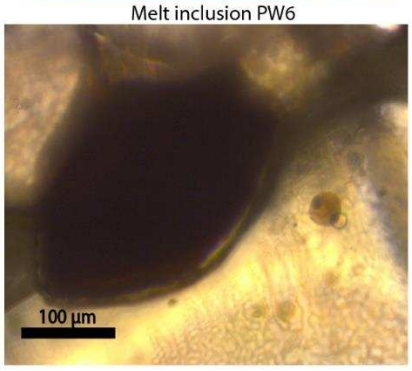

Melt inclusion PW10

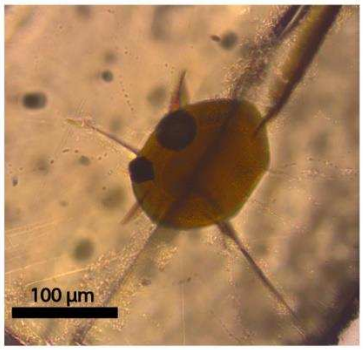

Melt inclusion PW11

Fig. S1. Images of melt inclusions analyzed in this study. All AVON3-71-2 melt inclusion images were taken after homogenization except for the image of melt inclusion AVON3-71-2-1. For melt inclusions PW-5 and PW-9a the images were taken post homogenization; the other eight Puu Wahi melt inclusions were not homogenized. Cracks in images resulted by grinding and polishing when exposing inclusions for analyses (i.e., cracks were not visible during or post-homogenization).

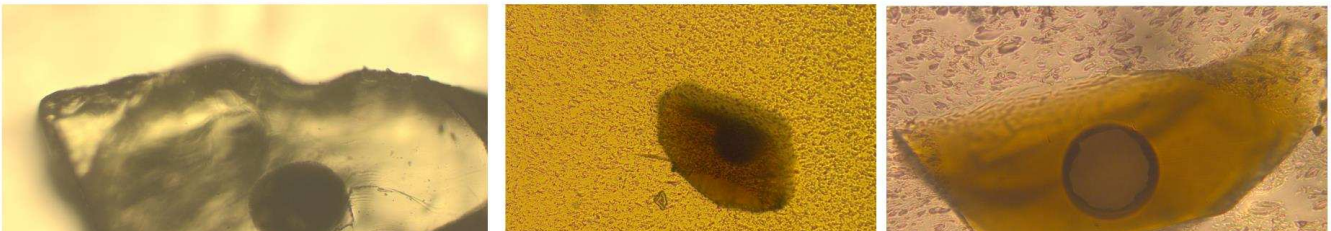

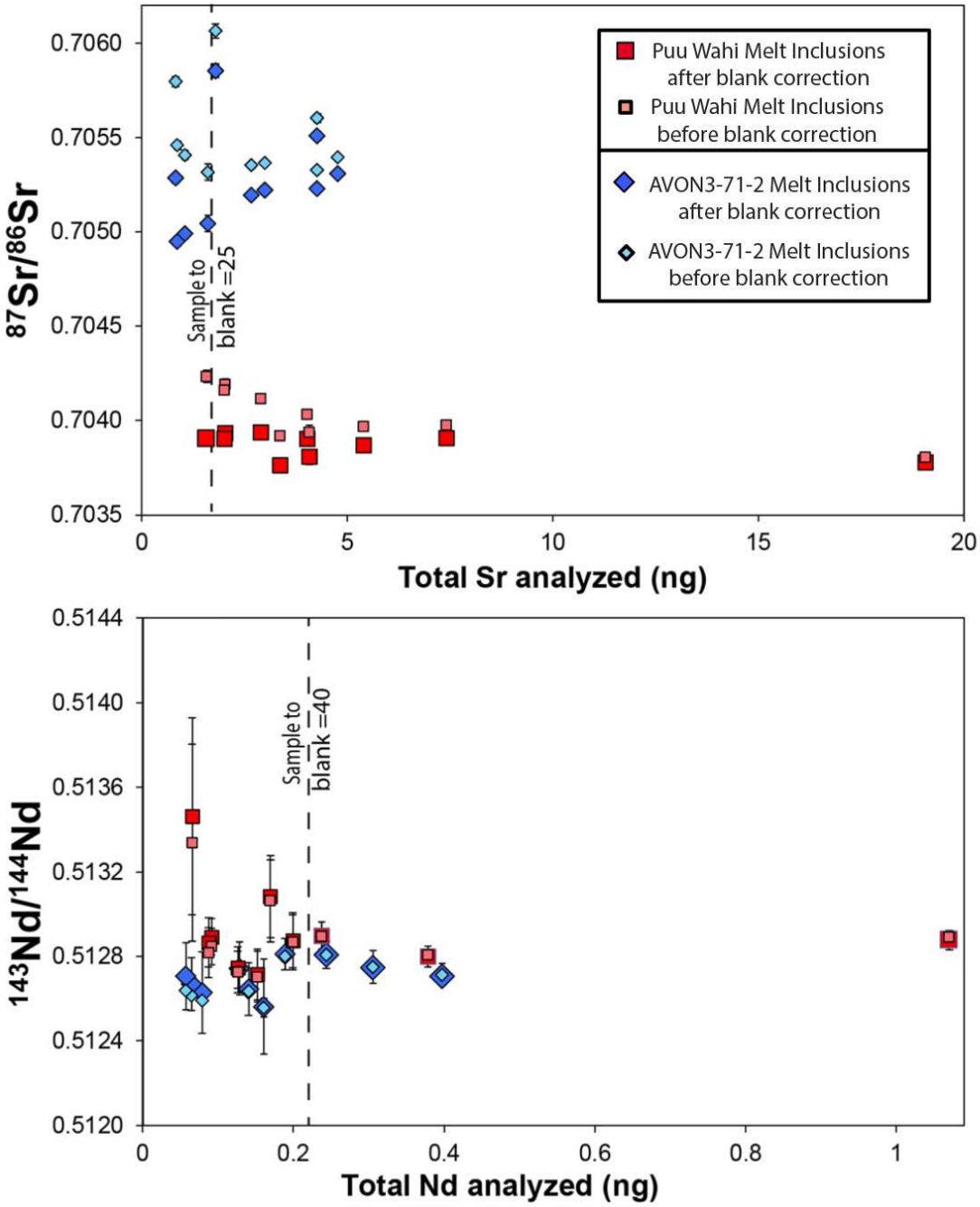

Fig. S2. Total Sr (nanograms) versus $^{87}Sr/^{86}Sr$ (top) and total Nd versus $^{143}Nd/^{144}Nd$ (bottom) for the melt inclusions analyzed in this study. For each sample there are two points plotted: the blank corrected ratio (darker red or blue) and the ratio before blank correction (lighter red or blue). The dashed vertical lines delineate the sample/blank thresholds for Sr (a ratio > 25) and Nd (> 40). Six melt inclusions had Nd_{sample}/Nd_{blank} ratios >40, and 15 melt inclusions Sr_{sample}/Sr_{blank} ratios > 25; all other melt inclusions had unacceptably low sample/blank ratios and were excluded from discussion in the text.

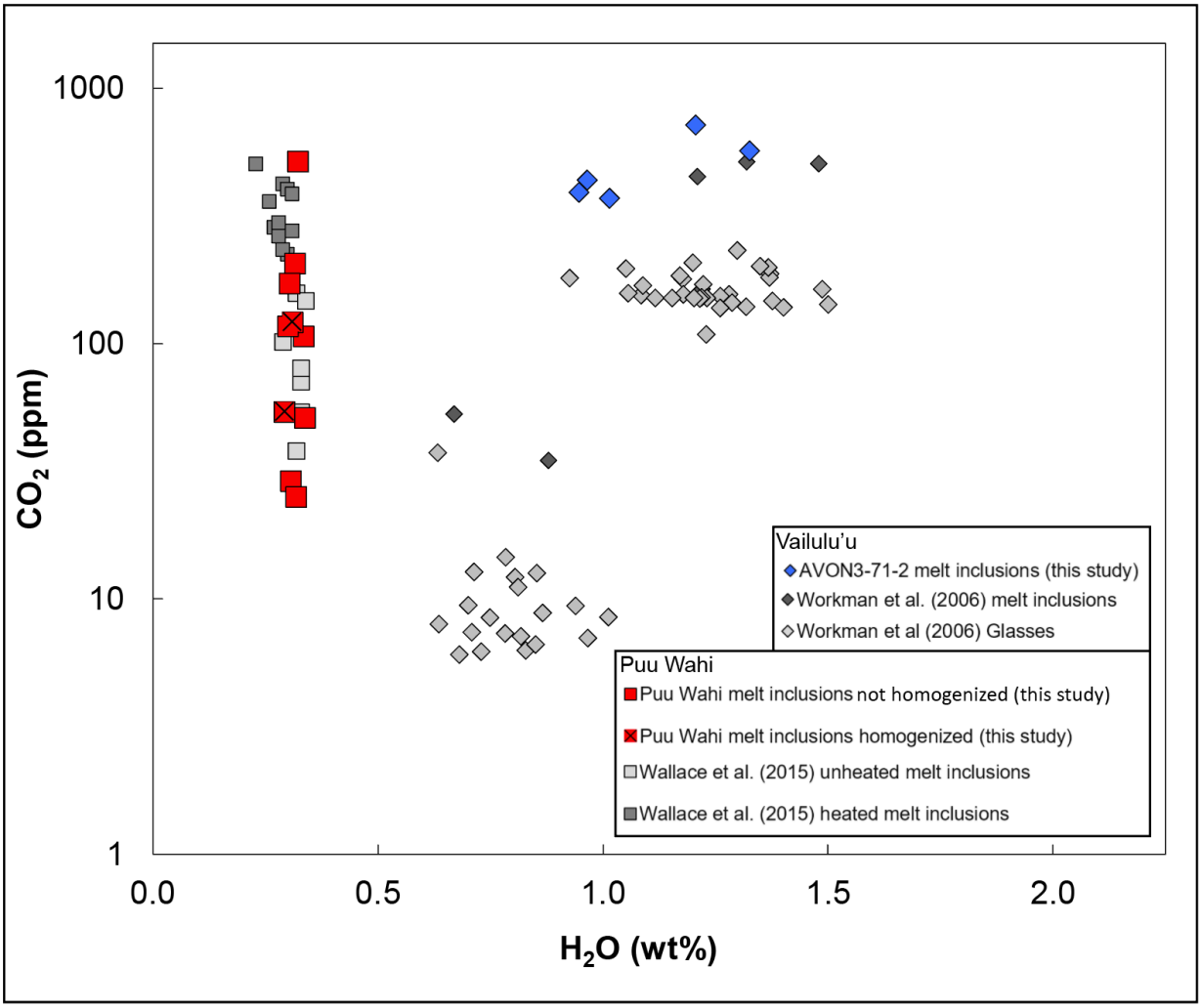

Fig. S3. CO_2 concentrations versus H_2O concentrations in the analyzed melt inclusions. Grey squares are Puu Wahi (Hawaii) melt inclusions analyzed for CO_2 and H_2O by Wallace et al. (2015), which show that a significant portion of the CO_2 in the melt inclusion resides in the vapor bubble. Wallace et al. (2015) analyzed two batches of melt inclusions from the same sample; one batch was unheated and a second batch was overheated then rapidly quenched to re-dissolve CO_2 before volatile analysis. Grey diamonds are Vailulu'u (Samoa) melt inclusions and submarine glasses reported in Workman et al. (2006); several of the Vailulu'u melt inclusions from Workman et al. (2006) have CO_2 and H_2O concentrations that are similar to the Vailulu'u melt inclusions examined here. Only two of the Puu Wahi melt inclusions required homogenization (PW5 and PW 9a), all AVON3-71-2 melt inclusions were homogenized.

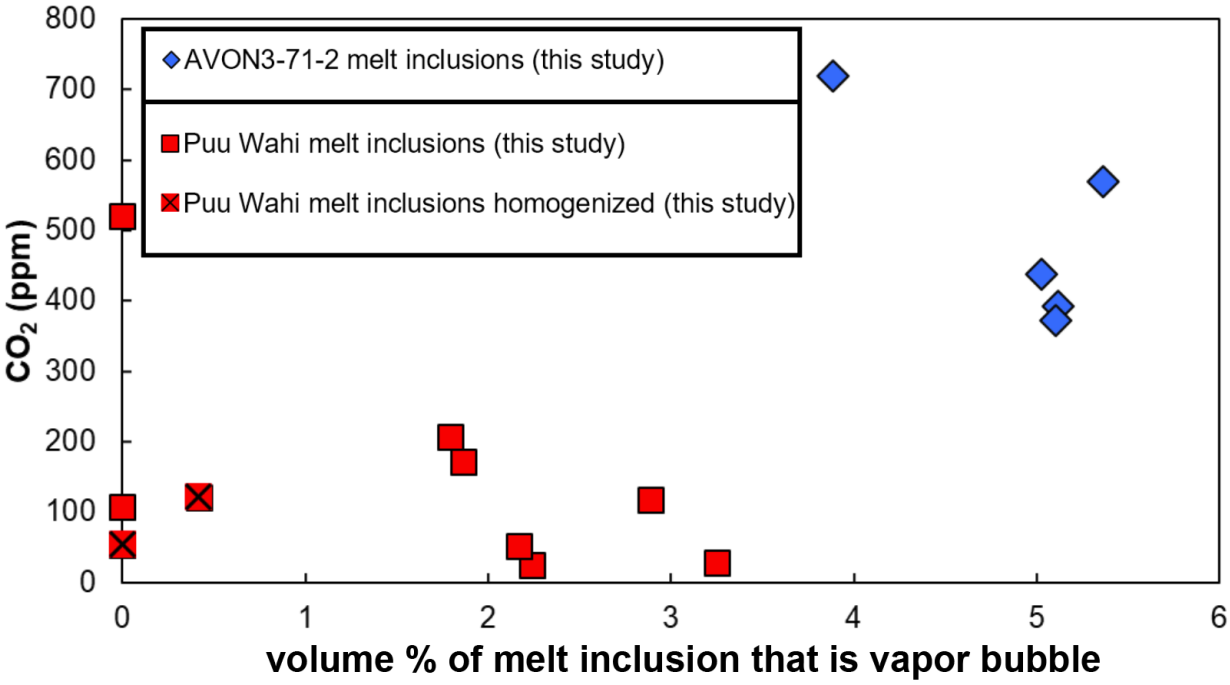

Fig. S4. The CO_2 concentration in the glassy melt inclusions plotted versus the percent of the melt inclusion volume that is vapor bubble. The red squares with an "X" represents the Puu Wahi melt inclusions that were homogenized. Four melt inclusions had no visible vapor bubble after homogenization and polishing and are therefore plotted as though 0% of melt inclusion volume was vapor bubble.

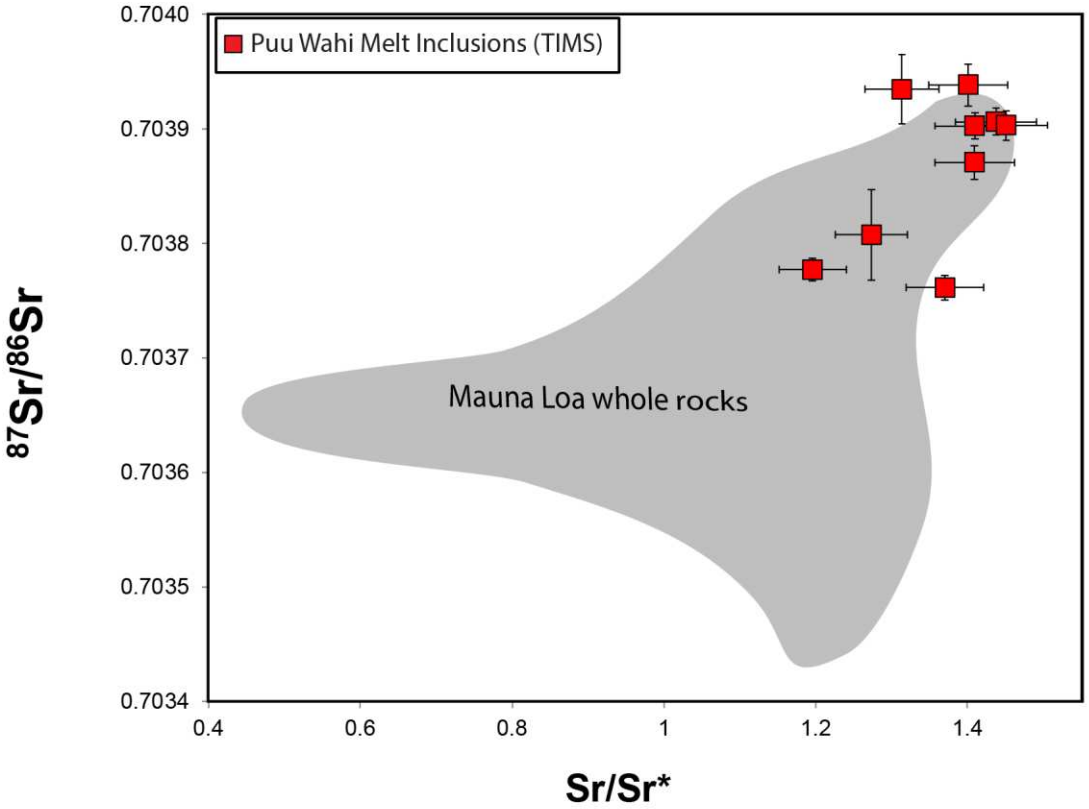
Puu Wahi Melt Inclusions (TIMS)
Mauna Loa whole rocks
0.7040
0.7039
0.7038
0.7037
0.7036
0.7035
0.7034
0.4
0.6
0.8
1
1.2
1.4
87Sr/86Sr
Sr/Sr*

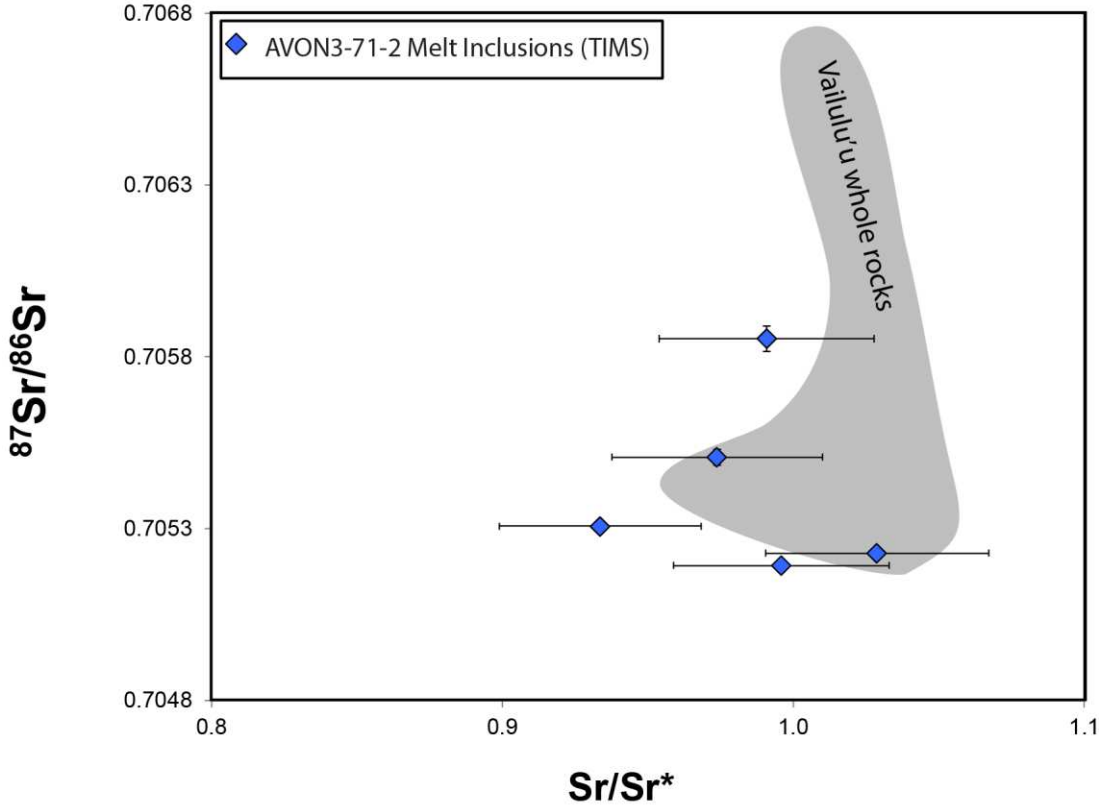
AVON3-71-2 Melt Inclusions (TIMS)
Vailulu'u whole rocks
0.7068
0.7063
0.7058
0.7053
0.7048
0.8
0.9
1.0
1.1
87Sr/86Sr
Sr/Sr*

Fig. S5. $^{87}Sr/^{86}Sr$ versus Sr/Sr* in the melt inclusions from Puu Wahi and AVON3-71-2. The Vailulu'u whole rock $^{87}Sr/^{86}Sr$ and Sr/Sr* field encompasses data from Workman et al. (2004), Jackson et al (2010), and Jackson et al. (2014). Mauna Loa whole rock $^{87}Sr/^{86}Sr$ and Sr/Sr* field encompasses data from the Jackson et al. (2012) compilation. $Sr/Sr^* = Sr_N/(Nd_N*Sm_N)^{0.5}$, where N represents normalization to primitive mantle concentrations from McDonough and Sun (1995).

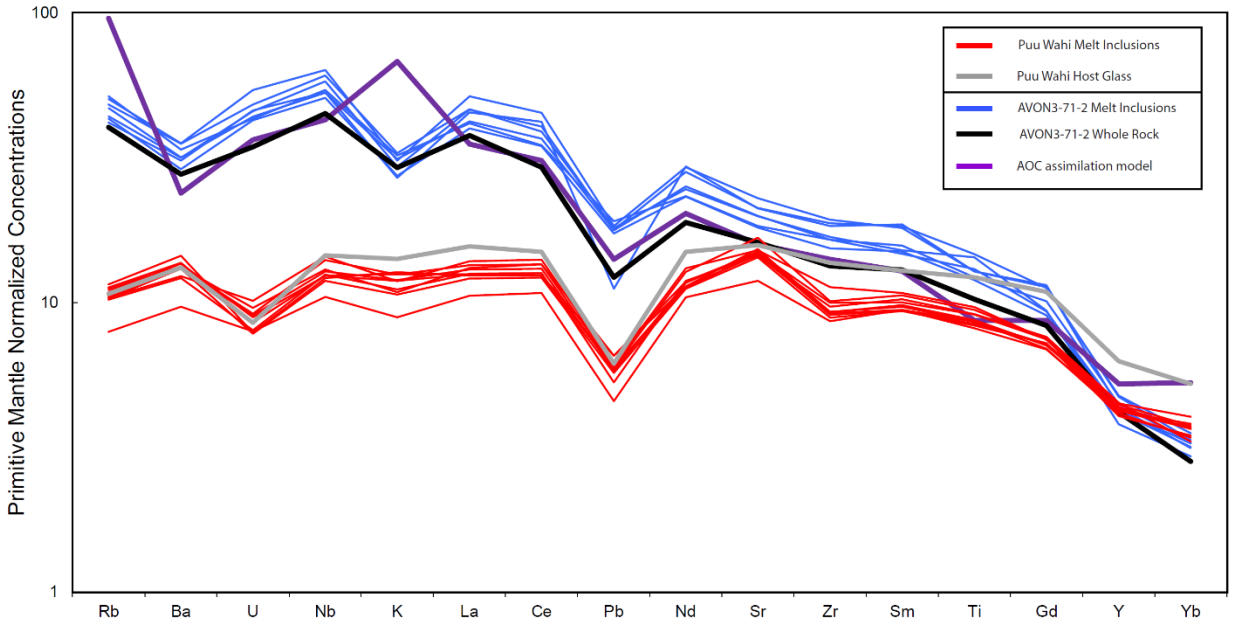

Fig. S6. Primitive mantle–normalized trace-element patterns from the seven glassy AVON3-71-2 melt inclusions and ten glassy Puu Wahi melt inclusions presented in this study (normalized to the primitive mantle values from McDonough and Sun, 1995). The black line is the trace-element data for the AVON3-71-2 whole rock from Workman et al. (2004), corrected for olivine accumulation to be in equilibrium with Fo_{90}. The grey line is the trace-element data for the host glass for the Puu Wahi olivines (Sobolev et al., 2011). The purple line is a model showing the result of the assimilation of 33% of the highest $^{87}Sr/^{86}Sr$ altered oceanic crust component from Hauff et al. (2003) (sample 801C 17R4 15-18 from ODP core 801) by the most depleted $^{87}Sr/^{86}Sr$ Vailulu'u melt inclusion (as discussed in the supplementary text).

References

Gale A., Dalton C. A., Langmuir C. H., Su Y., and Schilling J. 2013. The mean composition of ocean ridge basalts. Geochemistry, Geophysics, Geosystems **14**:489–518

Gao, R., Lassiter, J.C., Barnes, J.D., Clague, D.A., Bohrson, W.A., 2016. Geochemical investigation of Gabbroic Xenoliths from Hualalai Volcano: Implications for lower oceanic crust accretion and Hualalai Volcano magma storage system. Earth Planet. Sci. Lett., 442, 162-172.

Hart, S.R., Blusztajn, J., Dick, H.J.B., Meyer, P.S., Muehlenbachs, K., 1999. The fingerprint of seawater circulation in a 500-meter section of ocean crust gabbros. Geochim. Cosmochim. Acta 63, 4059–4080.

Hauff, F., Hoernle, K., Schmidt, A., 2003. Sr-Nd-Pb composition of Mesozoic Pacific oceanic crust (Site 1149 and 801, ODP Leg 185): Implications for alteration of ocean crust and the input into the Izu-Bonin-Mariana subduction system. Geochem. Geophys. Geosyst. 4, 8913 DOI:10.1029/2002GC000421

Hauri, E. H., Wang, J., Dixon, J.E., King, P.L., Mandeville, C., Newman, S., 2002. SIMS Investigations of volatiles in silicate glasses, 1: Calibration, matrix effects and comparisons with FTIR, Chem. Geol. 183, 99-114.

Jackson, M.G., Hart, S.R., Konter, J.P., Koppers, A.A.P., Staudigel, H., Kurz, M.D., Blusztajn, J., Sinton, J.M., 2010. The Samoan hotspot track on a "hotspot highway": Implications for mantle plumes and a deep Samoan mantle source. Geochem. Geophys. Geosyst. 11, Q12009, doi:10.1029/2010GC003232

Jackson M. G., Weis, D., Huang, S., 2012. Major element variations in Hawaiian shield lavas: source features and perspectives from global ocean island basalt (OIB) systematics. Geochem. Geophys. Geosyst. 13, Q09009. http://dx.doi.org/ 10.1029/2012GC004268

Jackson, M.G., Hart, S.R., Konter, J.G., Kurz, M.D., Blusztajn, J., Farley, K., 2014. Helium and lead isotopes reveal the geochemical geometry of the Samoan plume. Nature, 514, 355-358.

Jackson, M.G., Cabral, R.A., Rose-Koga, E.F., Koga, K.T., Price, A.A., Hauri, E.H., Michael, P., 2015. An ultra-depleted mantle component in the Ontong Java Plateau revealed by major, trace and volatile element abundances in olivine-hosted melt inclusions. Chem. Geol., 414, 124-137

Kelley, K.A., Plank, T., Ludden, J., Staudigel, H., 2003. Composition of altered oceanic crust at ODP Sites 801 and 1149. Geochemisty, Geophysics, Geosystems, 4, doi:10.1029/2002GC000435

Kumamoto, K. M., Warren, J.M., Hauri, E.H., 2017. New SIMS reference materials for measuring water in upper mantle minerals, Am. Mineral. 102, 537-547.

McDonough, W.F., Sun, S.S., 1995. The composition of the Earth. Chem. Geol. 120, 223–253

Moore, L. R., E. Gazel, R. Tuohy, A. S. Lloyd, R. Esposito, M. Steele-MacInnis, E. H. Hauri, P. J. Wallace, T. Plank, and R. J. Bodnar (2015), Bubbles matter: An assessment of the contribution of vapor bubbles to melt inclusion volatile budgets, American Mineralogist, 100(4), 806-823, doi:10.2138/am-2015-5036

Muller, R.D., Sdrolias, M., Gaina, C., Roest, W.R., 2008. Age, spreading rates, and spreading asymmetry of the world's ocean crust. Geochem., Geophys., Geosyst., 9, Q04006, doi:10.1029/2007GC001743

Peterson M. E., Saal A. E., Nakamura E., Kitagawa H., Kurz M., Koleszar A. M., 2014 Origin of the 'Ghost Plagiocalse' signature in Galapagos melt inclusions: New evidence from Pb isotopes. J. Petrol. 55(11), 2193–2216.

Rose-Koga E., Koga K., Hamada M., Helouis T., Whitehouse M.J., Shimizu N., 2014. Volatile (F and Cl) concentrations in Iwate olivine-hosted melt inclusions indicating low-temperature subduction. Earth Planets Space 66, 81. doi:10.1186/1880-5981-66-81.

Saal A. E., Kurz M. D., Hart S. R., Blusztajn J. S., Blichert-Toft J., Liang Y., Geist D. J., 2007. The role of lithospheric gabbros on the composition of Galapagos lavas. Earth Planet. Sci. Lett. 257, 391–406

Sano, T., Miyoshi, M., Ingle, S., Banerjee, N.R., Ishimoto, M., Fukuoka, T., 2008. Boron and chlorine contents of upper oceanic crust: Basement samples from IODP Hole 1256D. Geochem. Geophys. Geosyst., 9, Q12O15. doi:10.1029/2008GC002182

Simons, K., Dixon, J.E., Schilling, J.-G., Kingsley, R.H., Poreda, R., 2002. Volatiles in basaltic glasses from the Easter-Salas y Gómez Seamount Chain and Easter Microplate: Implications for geochemical cycling of volatile elements, Geochem. Geophys. Geosyst., 3(7), 1–29, doi:10.1029/2001GC000173.

Staudigel, H., Davies, G.R., Hart, S.R., Marchant, K.M., Smith, B.M., 1995. Large scale isotopic Sr, Nd and O isotopic anatomy of altered oceanic crust: DSDP/ODP sites 417/418. Earth Planet. Sci. Lett, 130, 169-185.

Staudigel, H., Plank, T., White, B., Schminke, H.-U., 1996. Geochemical fluxes during seafloor alteration of the basaltic upper oceanic crust: DSDP Sites 417 and 418, in Subduction: Top to Bottom, Geophys. Monogr. Ser., vol. 96, edited by G. E. Bebout et al., pp. 19-38, AGU, Washington, D.C., 1996.

Staudigel, H., 2003. Hydrothermal Alteration Processes in the Oceanic Crust. Treatise on Geochemistry, 3, 511-535.

Steele-MacInnis, M., Esposito, R., and Bodnar, R.J., 2011. Thermodynamic model for the effect of post-entrapment crystallization on the H2O-CO2 systematics of vapor-saturated, silicate melt inclusions. Journal of Petrology, 52, 2461–2482

Workman, R.K., Hart, S.R., Jackson, M.G., Regelous, M., Farley, K.A., Blusztajn, J., Kurz, M.D., 2004. Recycled metasomatised lithosphere as the origin of the Enriched Mantle II (EM2) end-member: Evidence from the Samoan Volcanic Chain. Geochem. Geophys. Geosys., 5, doi:10.1029/2003GC000623.

Workman, R.K., Hauri, E., Hart, S.R., Wang, J., Blusztajn, J., 2006. Volatile and trace elements in basaltic glasses from Samoa: Implications for water distribution in the mantle. Earth Planet. Sci. Lett., 241, 932–951.

Wallace, P.J., Kamenetsky, V.S., Cervantes, P., 2015. Melt inclusion CO2 contents, pressures of olivine crystallization, and the problem of shrinkage bubbles. Am. Mineral. 100 (4), 787–794.

Workman, R.K., Hauri, E., Hart, S.R., Wang, J., Blusztajn, J., 2006. Volatile and trace elements in basaltic glasses from Samoa: Implications for water distribution in the mantle. Earth Planet. Sci. Lett., 241, 932–951.